IEEE Access
Multidisciplinary | Rapid Review | Open Access Journal

Received April 20, 2021, accepted May 8, 2021, date of publication May 13, 2021, date of current version May 24, 2021.

Digital Object Identifier 10.1109/ACCESS.2021.3080086

Electronically Tunable ACO Based Fuzzy FOPID Controller for Effective Speed Control of Electric Vehicle

MARY ANN GEORGE[1], (Graduate Student Member, IEEE), DATTAGURU V. KAMAT[1], (Senior Member, IEEE), AND CIJI PEARL KURIAN[2], (Senior Member, IEEE)

[1]Department of Electronics and Communication Engineering, Manipal Institute of Technology, Manipal Academy of Higher Education (MAHE), Manipal 576104, India

[2]Department of Electrical and Electronics Engineering, Manipal Institute of Technology, Manipal Academy of Higher Education (MAHE), Manipal 576104, India

Corresponding author: Dattaguru V. Kamat (dv.kamath@manipal.edu)

ABSTRACT The phenomenal growth of the Electric Vehicle (EV) technology demands efficient and intelligent control strategies for the propulsion system. In this work, a novel fuzzy fractional order PID (FOPID) controller using Ant Colony Optimization (ACO) algorithm has been proposed to control EV speed effectively. The controller parameters and the fuzzy logic controller's membership functions are tuned and updated in real-time using the multi-objective ACO technique. The proposed controller's speed tracking performance is verified using the new European driving cycle (NEDC) test in the MATLAB-Simulink platform. The proposed controller outperforms the ACO-based fuzzy integer-order PID (IOPID), FOPID, and traditional IOPID controllers. The sensitivity analysis confirms the robustness of the proposed controller for varying parameters of the EV model. The stabilization of EV speed in the presence of external disturbance is also confirmed. In the proposed work, an attempt is made to analyze the system's stability using Matignon's theorem, considering the linearized EV model. The proposed controller gives optimum speed tracking performance compared to the Genetic Algorithm (GA) and the Particle Swarm Optimization (PSO) based fuzzy FOPID controllers. Additionally, the optimized fuzzy FOPID controller is realized using a second-generation current conveyor with extra inputs (EX-CCII) and fractional-order capacitors with electronic tunability. The controller circuit's performance evaluation is carried out in the Cadence Analog Design Environment using GPDK 180 nm CMOS process.

INDEX TERMS Ant colony optimization, electric vehicle, multi-objective optimization, fuzzy FOPID, second-generation current conveyor with extra inputs.

I. INTRODUCTION

The rise in environmental concerns and demand for fossil fuel resources has necessitated incorporating electric vehicle (EV) technology. In the recent past, EVs have gained popularity concerning their high efficiency, low maintenance cost, and easy operations [1], [2]. The emerging trend in EVs has led to massive pollution reduction and better sustainability in urban cities. The propulsion system has been an integral part in deciding the overall performance of EV. The researchers at industrial and academic levels have primarily focused on developing controls for the propulsion system of the EV [3]. Efficient performance and desirable energy management are the two key parameters that require intensive and focused investigations. The controller should provide the maximum speed with low tracking error and energy consumption [4]. The EV system is highly non-linear, time-dependent, and uncertain due to the varying road conditions, motor parameters, and external disturbances. Hence, designing a controller that eliminates the external disturbances and handling uncertainties with low control signal has become a challenge [5].

The conventional PID controllers are generally used in various industrial applications due to their simplicity and ease of tuning [6], [7]. However, they do not perform effectively at varied operating conditions and do not assure desired

The associate editor coordinating the review of this manuscript and approving it for publication was Haibin Sun.

dynamic performance [8]. The use of fuzzy logic control with PID controllers enhances the classical PID controller's performance with self-tuning features [9]–[13]. Fuzzy controllers have been widely used in controlling EV systems. Khatun *et al.* [14] developed a fuzzy controller to control the EV antilock braking system by compensating for the non-linear dynamics. A fault-tolerant fuzzy controller can raise EV's initial torque with variable characteristics of speed and high efficiency [15].

The emergence of fractional calculus has led to the development of fractional order PID controller that offers two additional degrees of freedom, the non-integer order of the integrator and the differentiator stages [16]–[18]. The non-integer order controller provided better servo, regulatory performance, and robustness compared to its integer-order counterparts. The significant benefits of fractional order controllers are their efficacy, flexibility in system modeling, and design performance [19], [20].

The artificial intelligence (AI) based controllers have gained importance due to their satisfactory performance in various motor control applications, including speed assessment and torque ripple minimization [21]. However, AI-based controllers suffer from drawbacks, such as large data requirements, extended learning, and training duration. A fuzzy logic controller is a powerful tool that can integrate human reasoning into the controller design [13]. The fuzzy controllers can operate in linear and non-linear systems without considering their accurate mathematical models [22]. The fuzzy controllers outperform other controllers in complex and non-linear systems for which good practical knowledge exists. The accuracy of fuzzy logic controllers depends on the type and number of fuzzy membership functions and fuzzy rules. At present, the optimization techniques explored with fuzzy logic control have gained massive attention in various industrial applications due to their high-quality results, high efficiency, ability to adapt, and high accuracy. Hence, an optimal fuzzy logic controller can be designed by utilizing optimization techniques such as Genetic Algorithm (GA) [23], Particle Swarm Optimization (PSO) [24], Backtracking Search Algorithm (BSA) [25], Bee Colony Optimization (BCA) and differential evolution (DE) [26].

Das *et al.* [27] presented a GA-based optimized fuzzy FOPID controller, which could provide a better set-point tracking with a significant compromise in rejecting the load disturbance. Kumar *et al.* [28] investigated the design of a cascade fractional-order fuzzy PI and PD controller for a hybrid electric vehicle based on a multi-objective genetic algorithm. The fuzzy FOPID controllers have been widely used in various applications such as vibration isolation structure [29], pneumatic pressure system [30], pumped storage unit regulating system [31], and Automatic Generation Control (AGC) for electrical power systems [8], [13]. It is evident from the literature that combining fuzzy logic with fractional operators could further improve the feedback control system's robustness. Additionally, introducing an adaptive or self-tuning feature can even enhance the controller capability and system performance.

The majority of the controllers in current industries have been implemented in the digital form using PLC or microprocessors. However, the digital controllers have low speed and low memory capacity, making them unsuitable for fast processes such as speed control of EVs and chemical reactions [32]. The digital implementation also suffers from high power consumption related to the analog-to-digital (A/D) converter.

There have been several works on the analog circuit realization of the FOPID controller reported in the literature, using analog blocks like Operational Transconductance Amplifier (OTA) [32], [33], CCII [34], Voltage Differencing Current Conveyor (VDCC) [35]. Most of these circuits suffer from drawbacks, such as a high number of active/ passive elements [32], [33], and lack of electronic tunability [34].

A. MOTIVATION AND RESEARCH GAP

The majority of the reported work on tuning the fuzzy logic input and output scaling factors focus on GA [23], PSO [23], [24], and Cuckoo algorithm [36]. Apart from the scaling factors, the position of the input and output membership functions plays a vital role in the fuzzy logic controller [37]. Hence, it is worth noting that the tuning of membership function can significantly enhance the system's performance.

The Ant Colony Optimization (ACO) algorithm is preferred to optimize the controller parameters and tune the membership functions due to its numerous advantages compared to other optimization algorithms such as GA and PSO [38]. The ACO algorithm is a meta-heuristic approach that offers high robustness, better reliability, greater flexibility, fast convergence, easy implementation, and fewer optimization parameters [38]–[41]. It is also capable of combining with other algorithms. It is well suited for feature selection and parameter tuning with better global search ability. It is suitable for dynamic applications and can quickly adapt to changes.

The analog circuit realization of the FOPID controller involves the realization of fractional-order capacitors, which are not yet available commercially. The behavior of the fractional-order capacitors can be emulated using the RC ladder/tree structures [42] and multiple-loop-feedback structures [43]. Considering the RC structures' greater energy consumption and a more significant number of active element count required for the multiple-loop-feedback structures, a better solution using a resistor less and energy-effective structure to realize the fractional-order capacitors is deemed necessary.

B. CONTRIBUTION AND PAPER ORGANIZATION

1. This work focuses on the efficient design and circuit realization of a fuzzy FOPID controller for EV speed control. The optimization of the input /output scaling factors, antecedent part of input membership function, and

coefficients of the consequent parts of the Takagi-Sugeno fuzzy inference system is performed using the ACO algorithm.
2. The proposed optimization is expected to minimize the multi-objective function to improve the time-domain performance indices. The novel controller's ability to reject disturbances and provide robustness to uncertainties and parameter variations has also been investigated in this study. The controller facilitates the fastest tracking with minimum overshoot and low values of time-domain performance indices.
3. The stability analysis and eigenvalue analysis of the proposed ACO-based fuzzy controller and EV model is carried out.
4. The performance of the proposed controller is also compared with GA and PSO-based fuzzy FOPID controllers.
5. The suggested controller is realized using a single EX-CCII, which provides a simultaneous realization of the fractional-order integrator and the differentiator stages of various orders and the unity gain frequencies. An OTA-based resistorless topology is employed to emulate the fractional-order capacitors used to realize the fractional-order differentiator and the integrator stages. This study anticipates gaining some valuable and novel insights into the effective real-time performance of the EV propulsion system to find broad applications in the ongoing efforts in sustainable growth.

The paper has been organized as follows: Section II describes the mathematical model of the EV. Section III gives the fuzzy FOPID controller structure with details of the two-dimensional rule base and membership functions. It also explains the formulation of a multi-objective function along with the ACO algorithm used for optimization. The circuit realization of the fuzzy FOPID controller using the EX-CCII with electronic tuning features is presented in Section IV. Section V compares the performances of the fuzzy IOPID and the fuzzy FOPID controllers for set-point tracking, disturbance rejection, and uncertainties. It also presents the results of circuit simulation, and the concluding remarks are outlined in Section VI.

II. MATHEMATICAL MODEL OF ELECTRIC VEHICLE

The EV mainly comprises a battery unit, controller, and electric motors connected to the vehicle through the transmission unit. The EV system dynamics has two parts: vehicle and motor dynamics. The electric vehicle system modeling involves the balancing of all the forces acting on a running vehicle. There are mainly four types of forces, namely rolling friction (F_{rr}), aerodynamic drag force (F_{ad}), gravitational force (F_g), and force due to vehicle acceleration (F_a), as shown in Figure 1.

Hence, the total traction force (F_t) acting on a vehicle is given by

$$F_t = F_{rr} + F_{ad} + F_g + F_a \tag{1a}$$

$$= \mu_{rr} mg + 0.5\rho A C_d v^2 + mg\sin\varphi + m\frac{dv}{dt} \tag{1b}$$

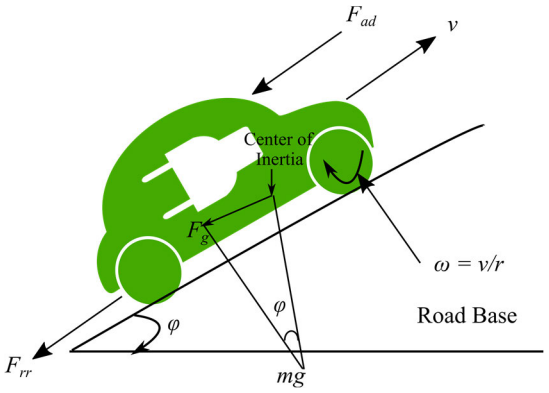

FIGURE 1. External forces acting on a running EV.

where m is the mass of the electric vehicle, g is the gravity acceleration, v the driving velocity of the vehicle, μ_{rr} the rolling resistance coefficient, ρ the air density, A the frontal area of the vehicle, C_d the drag coefficient and φ the hill-climbing angle. Table 1 describes the EV parameters and specifications.

TABLE 1. EV parameters and specifications [45].

Symbol	Value	Symbol	Value
$L_a + L_f$	6.008 mH	m	800 kg
$R_a + R_f$	0.12 Ω	A	1.8 m^2
L_{af}	1.766 mH	ρ	1.25 (kg/m^3)
i	78 A (250 max)	C_d	0.3
V	0 ~ 48 V	μ_{rr}	0.015
B	0.0002 N.M.s	φ	0°
J	0.05 kg m^2	G	11
ω	25 km/h	r	0.25 m

The resultant force F_t produces a torque T_L to the driving motor and is given by

$$T_L = F_t \times \frac{r}{G} \tag{2}$$

where r is the EV tire radius and G the gearing ratio.

The non-linear model of the DC motor [44] is given by

$$\frac{di}{dt} = \frac{1}{(L_a + L_f)}\left\{V - \left(R_a + R_f\right) i - L_{af} i\omega\right\} \tag{3a}$$

$$\frac{d\omega}{dt} = \frac{1}{J}\left\{L_{af} i^2 - B\omega - T_L\right\} \tag{3b}$$

where i is considered the armature and field current, ω the angular speed of the motor, L_a the armature inductance, R_a the armature resistance, L_f the field winding inductance, R_f the field winding resistance, L_{af} the mutual inductance among the field and armature windings, B the viscous coefficient, J the moment of inertia of the motor, T_L the external torque and V the input voltage.

Hence, the driving velocity of the vehicle v is given by

$$v = \omega \times \frac{r}{G} \tag{4}$$

Therefore, by combining the vehicle and the motor dynamics, the overall EV model is given by

$$\frac{di}{dt} = \frac{1}{(L_a + L_f)}\left\{V - \left(R_a + R_f\right) i - L_{af}\, i\omega\right\} \tag{5a}$$

$$\frac{d\omega}{dt} = \frac{1}{(J + m(r/G)^2)}\left\{L_{af}\, i^2 - B\omega - \frac{r}{G}\left(\mu_{rr} mg + 0.5\rho A C_d v^2 + mgsin\varphi\right)\right\} \tag{5b}$$

The equations (5a) and (5b) of the EV can be represented in Simulink, as shown in Figure 2.

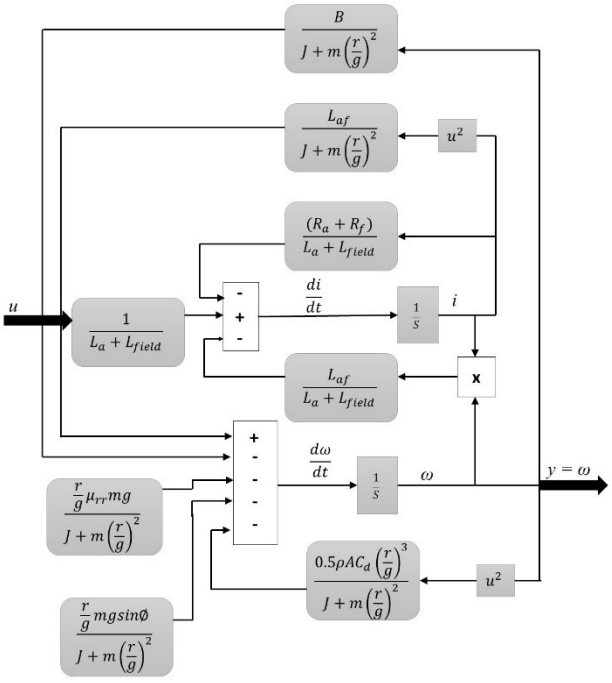

FIGURE 2. Representation of an EV system in Simulink.

The non-linear model in (5) can be converted into state-space form as

$$\dot{X} = f(X) + g(X)u \tag{6}$$

where

$$X = \begin{bmatrix} x_1 \\ x_2 \end{bmatrix} = \begin{bmatrix} i \\ \omega \end{bmatrix}$$

$$f(X) = \begin{bmatrix} -\dfrac{R_a + R_f}{L_a + L_f} x_1 - \dfrac{L_{af}}{L_a + L_f} x_1 x_2 \\ \dfrac{1}{J + m(r^2/G^2)}\left\{L_{af} x_1^2 - Bx_2 - \dfrac{r}{G}\left(\mu_{rr} mg + \dfrac{1}{2}\rho A C_d \dfrac{r^2}{G^2} x_2^2 + mgsin\varphi\right)\right\} \end{bmatrix}$$

$$g(X) = \begin{bmatrix} \frac{1}{L_a + L_f} \\ 0 \end{bmatrix}, \quad h(X) = x_2$$

III. DESIGN OF A FUZZY FRACTIONAL ORDER PID

During the last few decades, fractional calculus has been widely used in solving control problems [46]. Fractional calculus is an essential branch of mathematics that uses non-integer order powers of integration and differential operators.

The differ-integration operator ${}_\alpha D_t^r$ represents a fractional order differentiation and integration as in (7)

$${}_\alpha D_t^r \left\{ \begin{array}{r} \dfrac{d^r}{dt^r} r > 0 \\ 1 r = 0 \\ \int_\alpha^t (d\tau)^{-r} \; r < 0 \end{array} \right\} \tag{7}$$

where $r \in R$ is the order of the operation and α, t the lower and the upper limits.

Several definitions have been reported in the literature to define the differ-integration operator, such as Reimann-Liouville, Grunwald-Letnikov, Caputo, Cauchy integral formula. The fractional-order operator s^r can be approximated to an integer order rational function using Oustaloup's approximation method [47]. Oustaloup's method is based on a recursive distribution of poles and zeros for a frequency range of $[\omega_b, \omega_h]$. Oustaloup's approximation for the analog filter takes the form

$$s^r \cong C \prod_{k=-N}^{N} \frac{s + \omega_k'}{s + \omega_k} \tag{8a}$$

where $r \in [-1, 1] \subseteq R$

The expressions for zeros, poles and gain are given by

$$\omega_k' = \omega_b \left(\frac{\omega_h}{\omega_b}\right)^{\frac{k+N+0.5(1-r)}{2N+1}}$$

$$\omega_k = \omega_b \left(\frac{\omega_h}{\omega_b}\right)^{\frac{k+N+0.5(1+r)}{2N+1}} \tag{8b}$$

$$C = \omega_h^r \tag{8c}$$

Here, ω_b is the lower transitional frequency, and ω_h is the higher transitional frequency. The unity gain frequency ω_o is calculated by $\omega_o = \sqrt{\omega_b \omega_h}$ and order of the transfer function is $n = 2N+1$, which can only be an odd-order approximation. By selecting N = 2 and the frequency band as $[10^{-3}, 10^3]$, the analog filter order turns out to be equal to 5.

The expression of the FOPID controller is given as

$$C(s) = K_p + \frac{K_i}{s^\lambda} + K_d s^\mu \tag{9}$$

where K_p is the proportional gain, K_i the integral gain, K_d the derivative gain, λ the order of the integrator stage, and μ the order of the differentiator stage. The time-domain expression of the control output of the FOPID controller is given by

$$u(t) = K_p e(t) + K_i D^{-\lambda} e(t) + K_d D^\mu e(t) \tag{10}$$

where $e(t)$ is the tracking speed error.

The structure of a fuzzy FOPID controller is shown in Figure 3. The error (e) and the fractional derivative of error (de) are the two inputs to the fuzzy FOPID, and o is the output of the fuzzy FOPID controller.

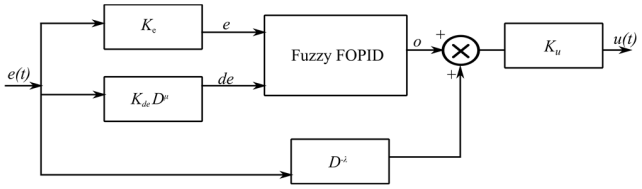

FIGURE 3. Structure of fuzzy FOPID controller.

By using linear transformation for the control output $u(t)$ in Figure 3, we get

$$u(t) = \left(K_e e(t) + K_{de} D^{\mu} e(t) + D^{-\lambda} e(t)\right) K_u \tag{11}$$

By comparing (10) and (11), the gain expressions can be given as

$$K_p = K_e K_u \tag{12a}$$
$$K_d = K_{de} K_u \tag{12b}$$
$$K_i = K_u \tag{12c}$$

where K_e, K_{de} are the input scaling factors and K_u the output scaling factor.

Here, a Takagi-Sugeno type fuzzy inference system (FIS) is used. The FIS has three blocks, i.e., fuzzification, decision-making logic with rule base, and defuzzification, as shown in Figure 4. In the fuzzification stage, the crisp input values are converted to a linguistic variable using a triangular membership function, with a 50% overlap. The triangular membership function is described as

$$f(x, a, b, c) = \begin{cases} 0, & x \le 0 \\ \dfrac{x - a_k}{b_k - a_k}, & a_k \le x \le b_k \\ \dfrac{c_k - x}{c_k - b_k}, & b_k \le x \le c_k \\ 0, & c_k \le x \end{cases} \tag{13}$$

where a_k, c_k denote the feet and b_k the peak of the triangular membership function. The distribution of membership functions for the input variables e and de are shown in Figures 5 (a) and 5 (b). The input variables have five fuzzy sets: Negative Big (NB), Negative Medium (NM), Zero (Z), Positive Medium (PM), and Positive Big (PB). Figure 6 shows the distribution of the output membership function. The fuzzy IF-THEN rule describes a condition that relates the linguistic variables and fuzzy sets to the

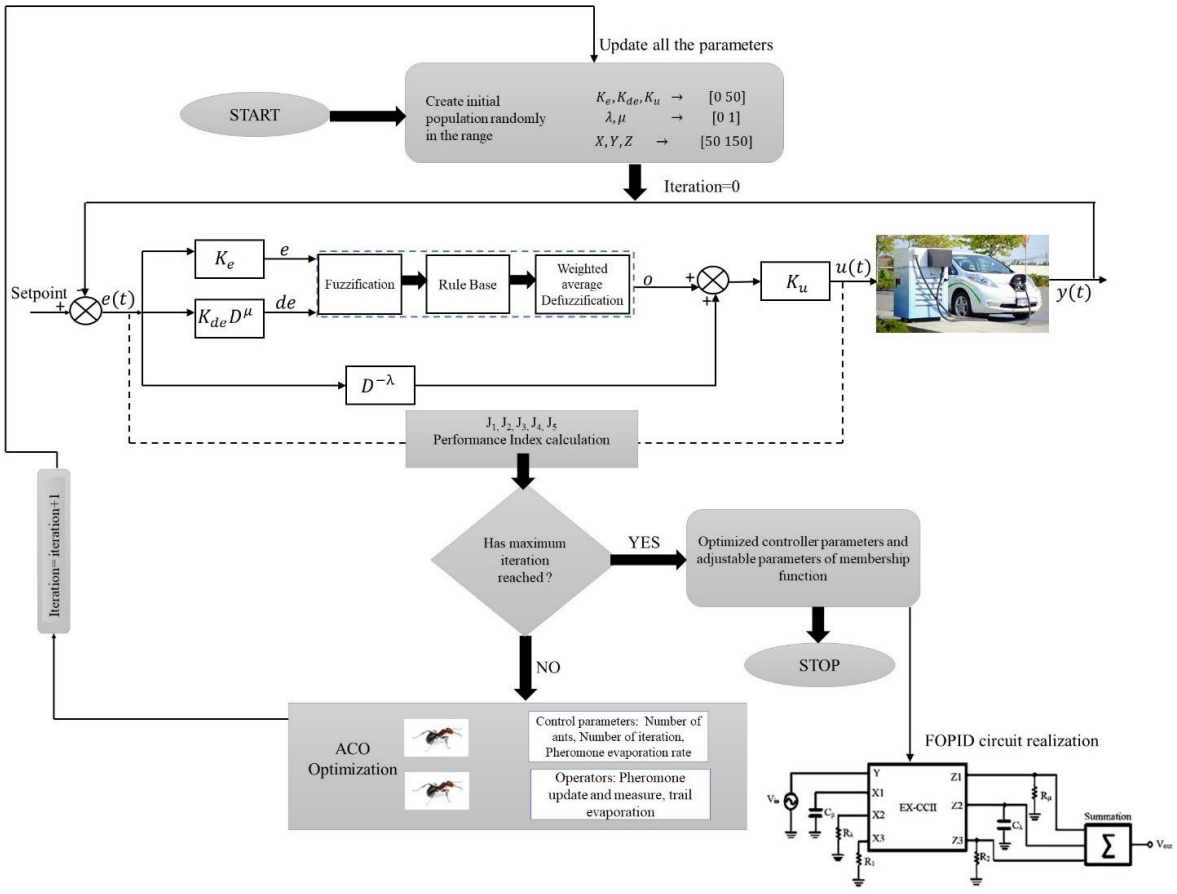

FIGURE 4. Block diagram of the proposed optimal fuzzy FOPID controller scheme for EV speed control.

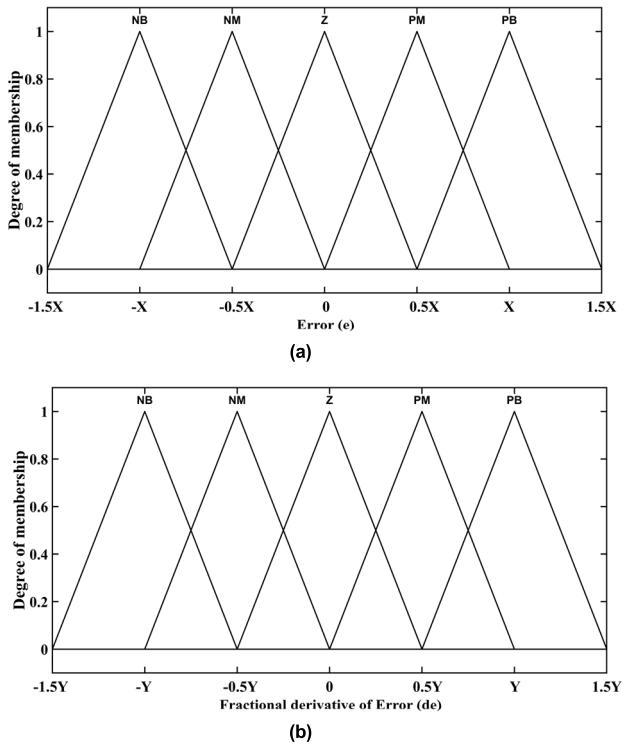

FIGURE 5. Distribution of input membership function (a) error (e), (b) fractional derivative of error (de).

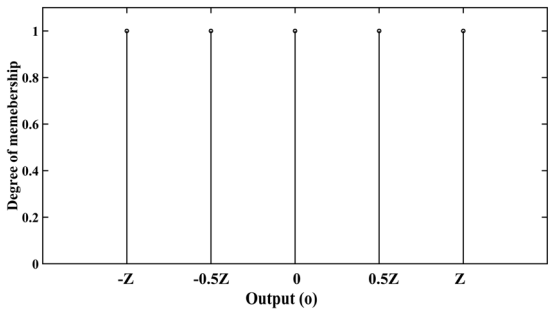

FIGURE 6. Distribution of the output of Takagi-Sugeno type FIS.

output [48]. Table 2 describes the 25 IF-THEN rules used in this work. The Takagi-Sugeno type FIS gives a crisp output, either a linear combination of the inputs or a constant. Hence, it is considered as a weighted average defuzzification process. The proposed scheme of the fuzzy FOPID controller for the EV system is illustrated in Figure 4. The Takagi-Sugeno FIS consumes less time compared to that of a Mamdani fuzzy system [9].

The input and output scaling factors (K_e, K_{de}, K_u), adjustable parameters of input membership function (X, Y), coefficient of the consequent part (Z), the order of integrator (λ), and order of differentiator (μ) are varied to achieve an optimal solution and improve the speed tracking performance of electric vehicle system.

The fuzzy FOPID controller is tuned using the ACO algorithm, and its performance is compared with other optimization algorithms in the MATLAB-Simulink platform.

TABLE 2. Rule base for fuzzy FOPID controller.

e/de	NB	NM	Z	PM	PB
NB	NB	NB	PM	NM	NM
NM	NB	NM	Z	Z	Z
Z	NB	NM	Z	PM	PB
PM	Z	Z	Z	PM	PB
PB	PM	PM	PM	PB	PB

A. ANT COLONY OPTIMIZATION (ACO)

The ACO is one of the robust and adaptive algorithms used to solve optimization problems based on the natural behavior of the ants [49]. The optimal solution can be determined when the ants' colony communicates with each other using an indirect method called the *pheromone decomposition*. The shortest distance from the initial state to the destination is found using a sequence of neighboring states. This algorithm can find the optimal solution faster when a higher number of pheromones are released. The pheromone matrix, which is used to determine the optimal solution, is $\psi = \psi_{ab}$. The initial state of the pheromone matrix is given by

$$\psi_{ab} = \psi_0 \quad \forall(a, b) \tag{14}$$

where $\psi_0 > 0$. The probability ($P^Y_{a.b}$) of selecting node a at node b is given as

$$P^Y_{a.b} = \frac{[\psi_{ab}(t)]^\alpha \, [\eta_{ab}]^\beta}{\sum_{a,b \in T^y} [\psi_{ab}(t)]^\alpha \, [\eta_{ab}]^\beta} \tag{15}$$

where T^y defines the path executed at a given time by an ant (Y), α and β are the constants that determine the relative impact of the pheromones and the heuristic factors on ants' decision. The heuristic factor η_{ab} is given by

$$\eta_{ab} = \frac{1}{distance\ between\ nodes\ a\ and\ b} \tag{16}$$

The quality of pheromone $\Delta\psi^Y_{ab}$ at each path is defined as

$$\Delta\psi^Y_{ab} = \begin{bmatrix} \frac{L^{best}}{L^Y} \\ 0 \end{bmatrix} \tag{17}$$

where L^{best} is the best solution in the current iteration and L^Y is the value of the objective function determined by an ant (Y).

A phenomenon known as pheromone evaporation is adopted to delete the previous pheromones when a better optimal solution is reached.

The expression for pheromone evaporation is given as

$$\psi_{ab}(t) = \rho\psi_{ab}(t-1) + \sum_{Y=1}^{NY} \Delta\psi^Y_{ab}(t) \tag{18}$$

where ρ ($0 < \rho \leq 1$) is the evaporation rate, and NY denotes the number of ants. Figure 7 shows the pseudocode for the ACO algorithm.

ACO Algorithm
Initialize the pheromone trail and parameters
Generate initial population size of ants
Evaluate the initial population according to fitness function
Find the best solution of the population
While not terminated
Do until each ant completely build a solution
Local trial update
End Do
Update the pheromone and probability
Evaporate the pheromones
Determine the best global ant
End while
Output the global best solution

FIGURE 7. Pseudocode for ACO algorithm.

B. FORMULATION OF OBJECTIVE FUNCTION FOR TUNING

A controller can be optimal when its control parameters are adjusted such that the cost function is minimized. In multi-objective optimization, the cost function is a weighted sum of two or more objective functions. During optimization, it is crucial to minimize both the error index and the control signal. This optimization type can reduce the control signal's value, preventing the actuator's integral wind-up and saturation. In this study, five performance indices have been considered as follows:

$$J_1 = ITSE + ISCO = \int_0^\infty te^2(t)dt + ISCO \quad (19a)$$

$$J_2 = ITAE + ISCO = \int_0^\infty t\,|e(t)|\,dt + ISCO \quad (19b)$$

$$J_3 = IAE + ISCO = \int_0^\infty |e(t)|\,dt + ISCO \quad (19c)$$

$$J_4 = ISE + ISCO = \int_0^\infty e^2(t)dt + ISCO \quad (19d)$$

$$J_5 = ITSE + ITAE + IAE + ISE + ISCO \quad (19e)$$

$$ISCO = \int_0^\infty u^2(t)dt \quad (19f)$$

where $e(t)$ is the error signal, $u(t)$ is the control signal, *ITSE* is the integral time square error, *ITAE* is the integral time absolute error, *IAE* is the integral absolute error, *ISE* is the integral square error, and *ISCO* is the integral of the squared control signal. Each of these performance indices has certain advantages in the control system design [50]. These performance indices are considered as the objective function for tuning, ensuring stability and better speed tracking performance when there is sudden load disturbance, parameter variation, and reference speed variation.

The ACO algorithm minimizes the objective function J_i ($i = 1, 2, 3, 4, 5$) to produce the optimally tuned input and output scaling factors, integral-differential orders, and adjustable parameters of membership functions of the fuzzy FOPID controller with a low control signal and error-index.

IV. REALIZATION OF FOPID CIRCUIT USING EX-CCII

The optimum fractional PID controller can be realized using the extra-X second-generation current conveyor (EX-CCII) [34]. The main advantage of this structure is that a single active element is used to realize the controller, and the fractional-order differentiator and the integrator stages of any order can be implemented using the structure, as shown in Figure 8.

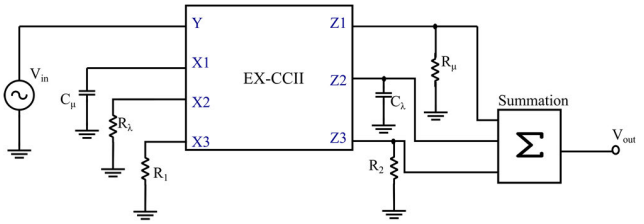

FIGURE 8. Realization of the FOPID controller using EX-CCII [34].

The terminal properties of EX-CCII are given by

$$\begin{aligned} V_{X1} &= V_{X2} = V_{X3} = V_Y \\ i_{Z1} &= i_{X1}, \quad i_{Z2} = i_{X2}, \; i_{Z3} = i_{X3} \\ R_Y &\to \infty \end{aligned} \quad (20)$$

where $V_{Xk}(k = 1, 2, 3)$ are the voltages at input terminals Xk, V_Y is the voltage at terminal Y, i_{Zk} $(k = 1, 2, 3)$ are the currents at terminal Zk and i_{Xk} $(k = 1, 2, 3)$ are the currents at terminals Xk.

The FOPID controller expression derived from applying terminal properties of EX-CCII in Figure 8 is given as

$$C(s) = \frac{R_2}{R_1} + \frac{1}{R_\lambda C_\lambda s^\lambda} + R_\mu C_\mu s^\mu \quad (21)$$

Here, C_λ and C_μ are the pseudo-capacitance with units $Farad/sec^{1-\lambda}$ and $Farad/sec^{1-\mu}$.

By comparing (21) and (9), we get

$$K_p = \frac{R_2}{R_1}, \quad K_i = \frac{1}{R_\lambda C_\lambda}, \; K_d = R_\mu C_\mu \quad (22)$$

The fractional-order capacitors are approximated using the modified Oustaloup's approximation and realized using the RC Valsa network, as shown in Figure 9.

The details of the multi-functional EX-CCII analog block and the three-input summation stage have been described in [34]. Figure 10 illustrates the CMOS realization of the three-input EX-CCII and the three-input summation stage. The EX-CCII circuit provides an accurate voltage conveying from terminal Y to terminals X1, X2, and X3. The currents from terminals X1, X2, and X3 are copied to terminals Z1, Z2, and Z3, respectively. The minimum supply voltage required is $V_{THn}+2V_{DS,sat}$.

As the EX-CCII analog blocks are not available commercially, the FOPID controller circuit can be realized using CCII/ CFOA integrated circuit (IC) AD844, as shown in Figure 11.

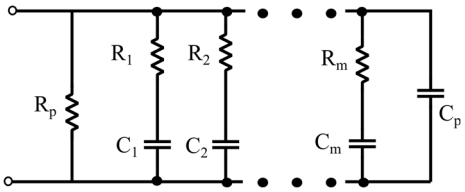

FIGURE 9. Valsa RC network.

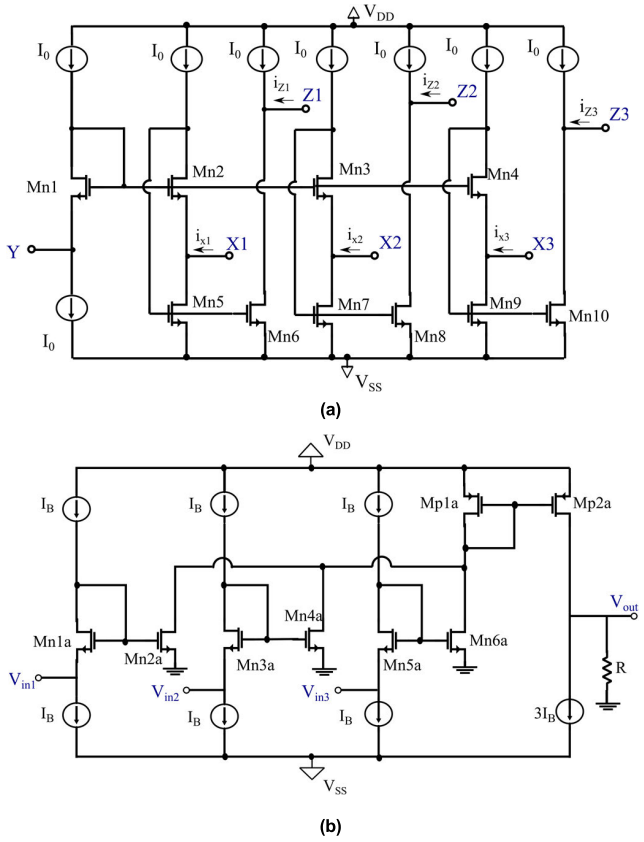

FIGURE 10. CMOS circuit of (a) three input EX-CCII, (b) three input summation stage [34].

The output expression for the summation stage, shown in Figure 10 (b), is given as

$$V_{out} = g_m R(V_{in1} + V_{in2} + V_{in3}) \tag{23}$$

Here, g_m is the transconductance of the transistors Mn1a-Mn6a and the resistance $R = 1/g_m$.

The electronic tunability of the EX-CCII based FOPID controller circuit in Figure 8 can be achieved by replacing all the passive grounded and floating resistors using operational transconductance amplifier (OTA) simulated resistors [51], [52], as shown in Figure 12 (a) and (b), respectively. This circuit offers benefits such as electronic tunability, wide bandwidth, simple design, and a wide range of resistance between 50 MΩ and 1 kΩ.

Assuming matched transistors, in Figure 12, the expression for current I_1 is given by

$$I_1 = -I_2 = G_m(V_1 - V_2) \tag{24}$$

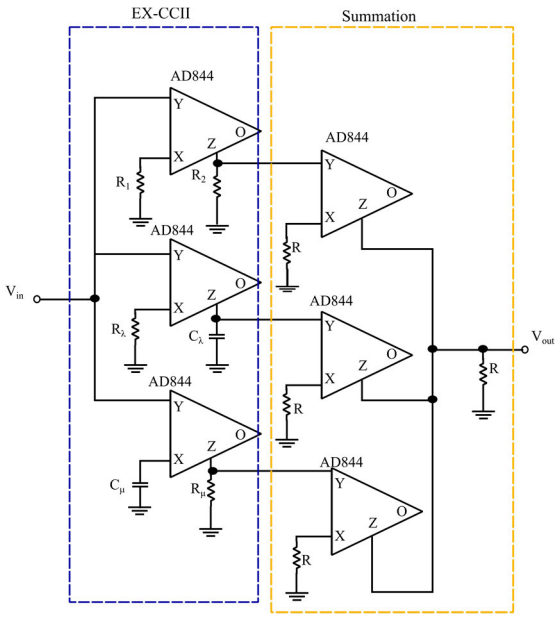

FIGURE 11. FOPID controller circuit using IC AD844 (current feedback operational amplifier).

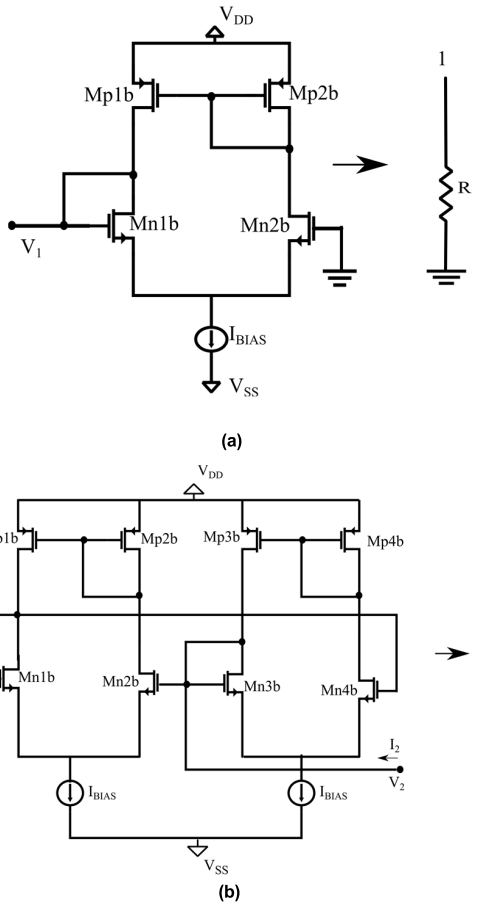

FIGURE 12. CMOS circuit of an electronically tunable resistor using OTA (a) grounded type, (b) floating type.

where V_1, V_2 are the input voltages of the transconductance amplifier and G_m is the transconductance.

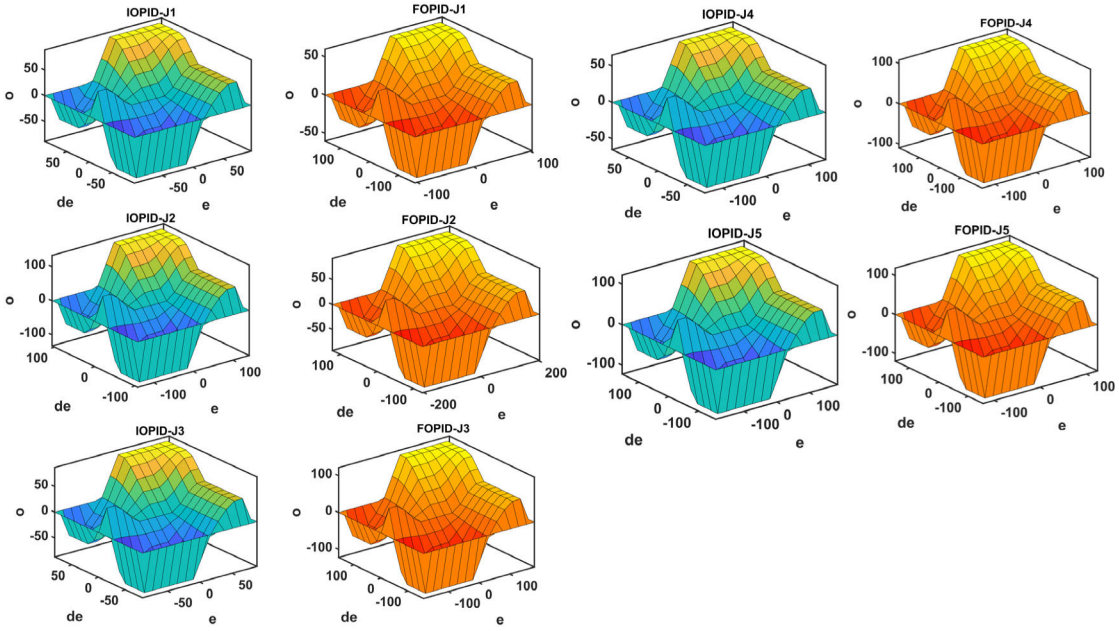

FIGURE 13. Output surface of fuzzy FOPID and IOPID controllers after ACO using J_1, J_2, J_3, J_4, and J_5 objective functions.

The resistance R and R_{12} can be found as

$$R = \frac{V_1}{I_1} = \frac{1}{\sqrt{\beta I_{Bias}}} \tag{25a}$$

$$R_{12} = \frac{V_1 - V_2}{I_1} = \frac{V_2 - V_1}{I_2} = \frac{1}{\sqrt{\beta I_{Bias}}} \tag{25b}$$

where I_{Bias} is the input biasing current β is the transconductance parameter of the MOS differential pair.

V. RESULTS AND DISCUSSION

The optimal fuzzy FOPID controller for EV speed control shown in Fig. 4 is simulated using MATLAB-Simulink and Cadence Virtuoso Analog Design Environment. This section demonstrates the superiority of the ACO-based fuzzy FOPID controller over fuzzy IOPID controller, FOPID, and conventional IOPID controller through simulation of the EV system's speed tracking performance.

The parameters selected for ACO are given in Table 3. The ACO minimizes the objective function (19a)-(19e) to determine the fuzzy controllers' optimal control parameters. Table 4 shows the fuzzy FOPID and fuzzy IOPID controller parameters obtained after optimization considering various objective functions. Here, *X, Y* are the antecedent values, and *Z* the value of the consequent.

Figure 13 illustrates the non-linear surface plot of the fuzzy IOPID and fuzzy FOPID obtained after ACO by minimizing the J_1, J_2, J_3, J_4, J_5 objective functions. It shows the input and output relationship of the fuzzy logic controller. Here, the three axes are the error (e), the fractional derivative of error (*de*), and the output (o) of the Takagi-Sugeno FIS. It illustrates that the distribution of *e, de*, and the coefficient of the consequent part of the output varies during the optimization. The blue and orange colour plots represent the output surface plot of fuzzy IOPID and fuzzy FOPID, respectively.

TABLE 3. Parameters for ACO.

Parameter	Value
Iteration	100
No. of ants	100
α	0.8
β	0.2
ρ	0.7
Population	100
K_e, K_{de}, K_u	[0 50]
λ, μ	[0 1]
X, Y, Z	[50 150]

Four operating scenarios are considered to validate the effectiveness and robustness of the proposed controllers, namely set-point tracking, disturbance rejection, noise suppression, and sensitivity analysis. This section also presents the stability analysis and eigenvalue analysis of the EV system. The performance comparison of the proposed scheme with other existing controllers is also described in this section.

a. Set-Point Tracking: The New European Driving Cycle (NEDC) test is performed to validate the fuzzy FOPID controller's performance. The NEDC has been commonly used to test the light-weighted EVs in Europe and India [53]. The maximum speed of the NEDC cycle is 120 km/h, as shown in Figure 14. The proposed fuzzy FOPID controller and fuzzy IOPID controller's performance to track the NEDC test is compared and illustrated in Figure 15 (a). It also shows

TABLE 4. Optimal set of tuning parameters for fuzzy FOPID and fuzzy IOPID controllers with ACO.

Controller	Objective function	K_e	K_{de}	K_u	λ	μ	X	Y	Z
Fuzzy IOPID	J_1	46.50	16.98	48.95	1	1	64.51	66.11	89.63
	J_2	20.62	13.03	43.91	1	1	94.44	71.02	133.18
	J_3	28.72	23.52	29.17	1	1	59.80	55.60	87.83
	J_4	46.55	28.62	47.40	1	1	94.44	53.13	65.91
	J_5	46.05	39.01	33.76	1	1	124.47	105.05	122.80
Fuzzy FOPID	J_1	4.696	28.27	41.45	0.66	0.59	69.81	104.65	60.91
	J_2	21.01	38.01	37.02	0.54	0.52	136.68	82.83	92.24
	J_3	1.99	45.25	37.91	0.45	0.64	120.87	105.15	52.20
	J_4	49.65	41.15	47.70	0.39	0.87	88.13	133.18	109.06
	J_5	1.64	33.61	24.17	0.86	0.35	83.83	100.65	119.07

TABLE 5. Performance parameters for fuzzy FOPID and IOPID controllers.

Controller	Objective function	Settling time (sec)	Rise time (sec)	Overshoot (%)	Steady-State error	*ITSE*	*ITAE*	*IAE*	*ISE*	Total indices
Fuzzy IOPID	J_1	1.00	0.595	0.707	0.0008	0.06	9.573	0.626	0.22	10.49
	J_2	9.48	1.04	2.28	0.0012	0.20	12.32	1.15	0.390	14.06
	J_3	8.51	1.45	2.04	0.0009	0.306	19.39	1.429	0.464	21.59
	J_4	3.80	1.66	1.25	0.002	0.318	24.04	1.445	0.451	26.25
	J_5	2.02	1.17	0.91	0.0015	0.165	17.06	1.05	0.33	18.61
Fuzzy FOPID	J_1	0.83	0.16	0.502	0.0011	0.04	8.83	0.49	0.107	9.46
	J_2	1.39	0.14	0.520	0.0018	0.04	10.45	0.465	0.115	11.07
	J_3	0.71	0.13	0.510	0.0008	0.22	8.45	0.808	0.228	9.71
	J_4	3.35	0.26	0.505	0.0009	0.133	6.028	0.814	0.27	7.25
	J_5	**0.75**	**0.081**	**0.505**	**0.0001**	**0.006**	**5.129**	**0.192**	**0.03**	**5.36**

the speed tracking performance of an ACO-based IOPID and FOPID controller. The proposed controllers' effectiveness is demonstrated by plotting the error signals and controller effort for each controller, as shown in Figure 15 (b) and 15 (c), respectively. As it can be inferred, while the IOPID controller produces the highest control effort and error signal, fuzzy FOPID generates the lowest control effort and error signal making its performance superior to others.

Table 5 summarizes the performance parameters of fuzzy FOPID and fuzzy IOPID controllers for various objective functions. The time-domain specifications such as settling time, rise time, percentage overshoot, steady-state error, and the performance indices such as *ITSE*, *ITAE*, *IAE*, *ISE*, and J_5 are compared for both controllers. Critical examination reveals that the fuzzy FOPID controllers' performance is far better than the fuzzy IOPID controllers with high accuracy, less settling time, percentage overshoot, steady-state error, and error indices. It also shows that the J_5 optimized controllers have superior performance compared to J_1, J_2, J_3, and J_4 optimized controllers.

The multi-objective optimization can result in solutions called the Pareto optimal solutions or non-dominant solutions. Figure 16 shows the distribution of the non-dominant solutions in the 4-dimensional Pareto optimal front (*ITAE, IAE, ITSE, ISE*) using multi-objective ACO. Here, J_5 multi-objective function is chosen, and the resulting convergence graph of multi-objective ACO for 100 generations is illustrated in Figure 17.

b. Disturbance Rejection: The robustness and the effectiveness of the fuzzy FOPID controller are verified in actual working conditions by introducing disturbances. An efficient and robust controller must reject the disturbance such that the deviation from the desired response is minimum. The speed tracking performance of the suggested controllers under the influence of disturbance is shown in Figure 18. The results show that the ACO-based IOPID and the FOPID cannot

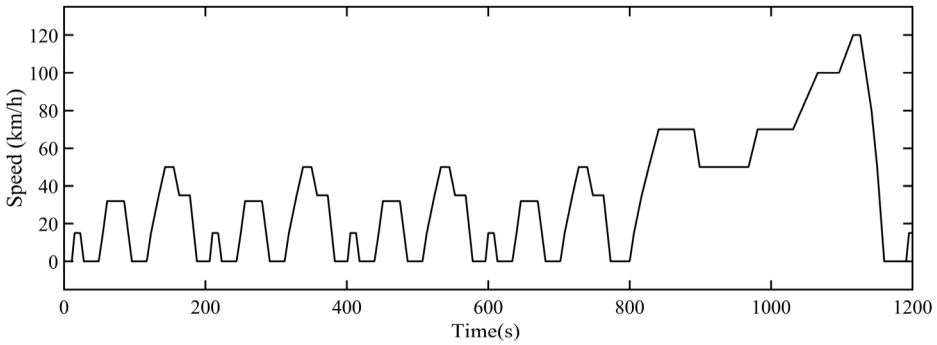

FIGURE 14. New European drive cycle.

accurately track the NEDC cycle than the fuzzy-based controllers. The fuzzy-based controllers can return to the set-point value quickly after the appearance of external disturbance. Also, such a system requires less recovery time compared to others.

c. Noise suppression: The EV system's robustness in the presence of measurement noise is tested by introducing a random signal of amplitude -0.04 to +0.04 and sampling time 0.01 seconds. Figure 19 demonstrates the effects of adding the noise input to the system. The fuzzy FOPID gives relatively minor fluctuation than fuzzy IOPID, FOPID, and IOPID controllers, showing a superior and robust control performance in noise suppression.

d. Sensitivity Analysis and Robustness: The controllers' robustness is demonstrated by introducing uncertainties and varying EV system parameters. Here, the uncertain parameters of the EV like mass (m), drag coefficient (C_d), rolling resistance coefficient (μ_{rr}) and EV tire radius (r) are varied, and the percentage of variation in these parameters is shown in Table 6. Figure 20 shows the robustness of the suggested controllers against the variations in system parameters, i.e., change in m by $+30\%$, μ_{rr} by $+30\%$, C_d by -20% and r by $+25\%$. It is observed that, compared to other controllers, the fuzzy FOPID controller takes the minimum time to complete the full power acceleration and stabilize in the presence of the uncertainties.

The critical frequency domain specifications are [54]:

Sensitivity function

$$S(s) = \frac{1}{1 + L(s)} \tag{26a}$$

Complementary Sensitivity function

$$T(s) = \frac{L(s)}{1 + L(s)} \tag{26b}$$

Disturbance Sensitivity

$$S_d(s) = \frac{G(s)}{1 + L(s)} \tag{26c}$$

Control Sensitivity

$$S_u(s) = \frac{C(s)}{1 + L(s)} \tag{26d}$$

TABLE 6. Uncertain parameters Of EV system.

Parameter	Variation %
$R_a + R_f$	+10
$L_a + L_f$	-20
r	+25
J	-20
m	+30
C_d	-20
μ_{rr}	+30

where $G(s)$ is the plant transfer function, $C(s)$ indicates the controller transfer function, and $L(s) = G(s)C(s)$ represents the loop transfer function.

The sensitivity function shows the system's ability to suppress load disturbances and attain good set-point tracking. The complementary sensitivity function specifies the robustness against the measurement noise [54]. The frequency-domain plots of sensitivity function, complementary sensitivity function, disturbance sensitivity, and control sensitivity are shown in Figure 21. For satisfactory system performance, the sensitivity function must have a small value at lower frequencies, and the complementary sensitivity function must have a small value at higher frequencies. The plots show that the fuzzy FOPID controller provides a better load disturbance rejection and a better high-frequency measurement noise rejection than other controllers. It is also observed that the sensitivity peak under fuzzy FOPID controller is minimum, while the conventional IOPID and FOPID controllers have higher sensitivity peaks.

e. Matignon's Theorem and Stability Analysis:

Theorem: The fractional-order transfer function $G(s) = N(s)/D(s)$ is stable in s-plane if and only if the following condition is satisfied [55]:

$$|arg(w_i)| > q\frac{\pi}{2}, \quad \forall w_i \in C, \tag{27}$$

the i$^{\text{th}}$ root of $D(w) = 0$, where $w = s^q$, $(0 < q < 2)$.

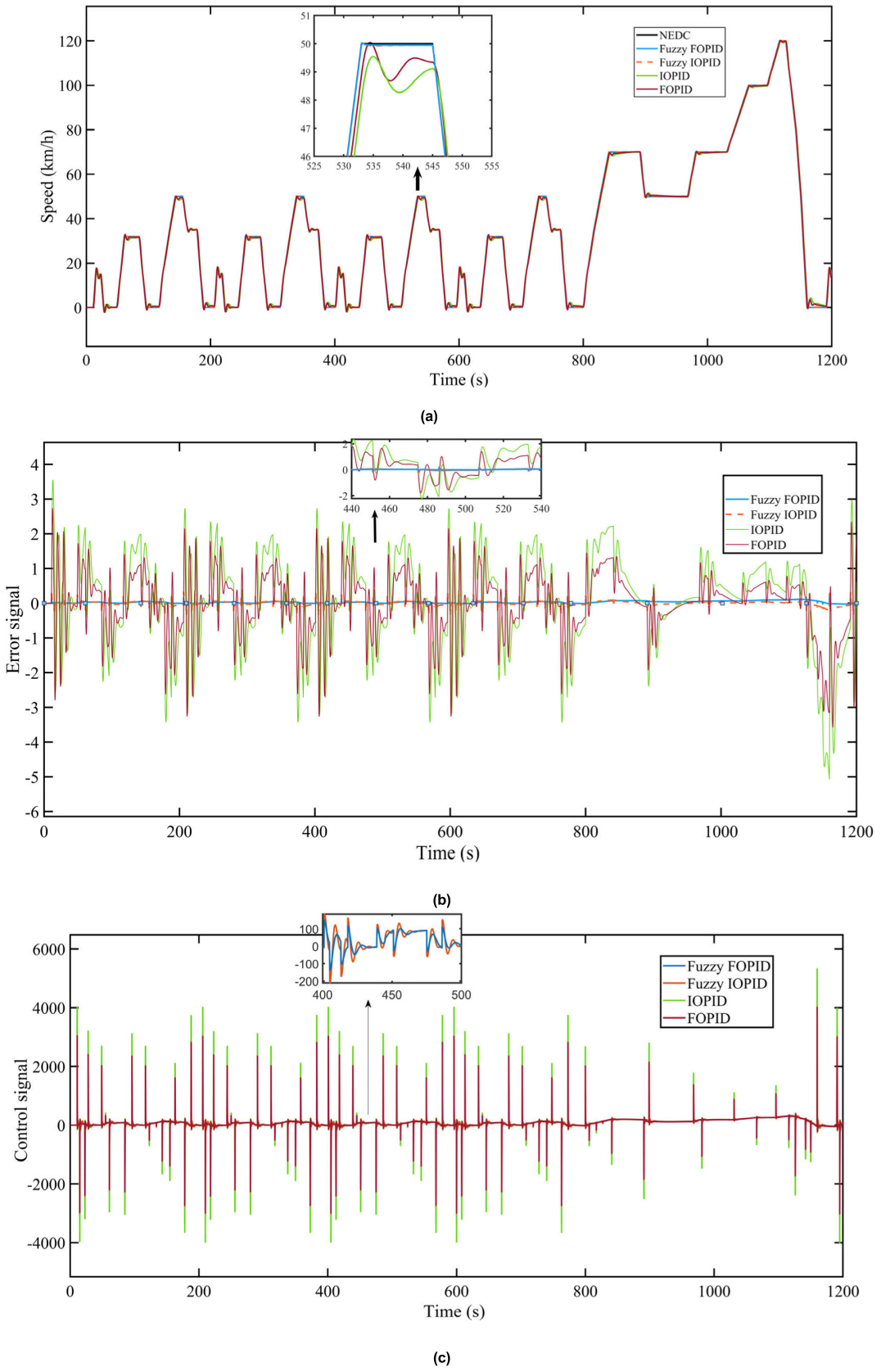

FIGURE 15. Performance of fuzzy FOPID, fuzzy IOPID, FOPID, and IOPID (a) to track NEDC speed test, (b) error signal, (c) controller effort.

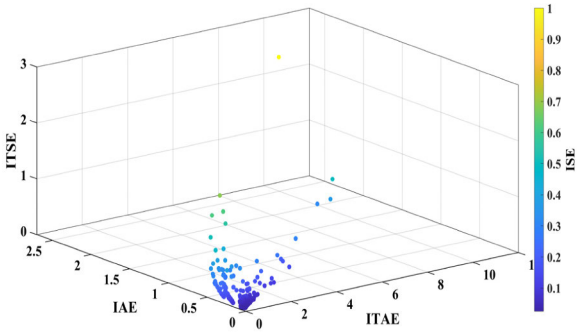

(a)

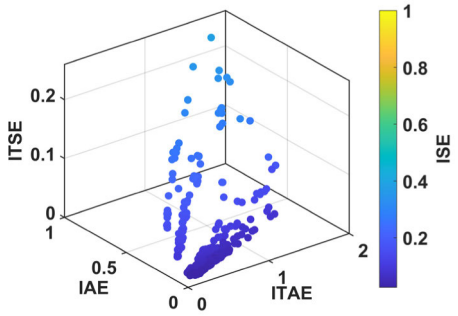

(b)

FIGURE 16. (a) 4D Pareto front using multi-objective ACO, (b) Zoomed plot.

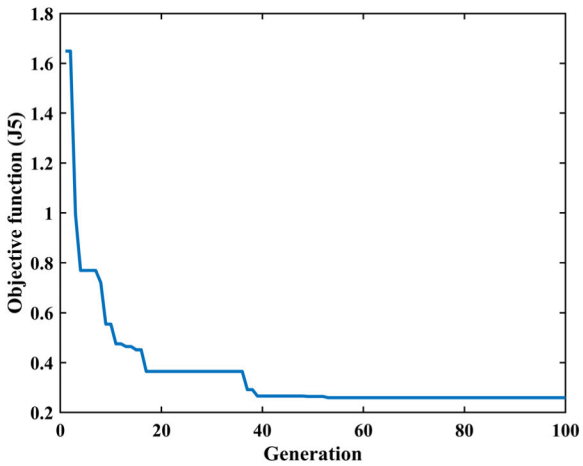

FIGURE 17. Convergence graph of ACO.

The linearized model of the EV system, which is obtained using system identification, is given by

$$G(s) = \frac{\left\{\begin{array}{c} 0.01292s^3 + 0.005944s^2 \\ +0.0004034s + 1.836e-05 \end{array}\right\}}{\left\{\begin{array}{c} s^5 + 0.2985s^4 + 0.1139s^3 \\ +0.01532s^2 + 0.001381s + 4.641e-05 \end{array}\right\}} \tag{28}$$

Here, one set of the ACO based fuzzy controller parameters is considered, i.e., $K_u = 23.15$, $K_e = 1.69$, $K_{ce} = 13.78$, $\lambda = 0.514$ and $\mu = 0.902$.

Hence, the expression of the FOPID controller takes the form

$$C(s) = 39.12 + \frac{23.15}{s^{0.514}} + 319s^{0.902} \tag{29}$$

Hence, the characteristic equation of the system is given as

$$\begin{aligned} 1 + G(s)\,C(s) = 0 \\ s^{5.514} + 0.2985s^{4.514} + 4.1151s^{4.416} + 0.61855s^{3.514} \\ + 1.8961s^{3.416} + 0.29863s^3 + 0.24785s^{2.514} \\ + 0.12868s^{2.416} + 0.1376s^2 + 0.017162s^{1.514} \\ + 0.0058568s^{1.416} + 0.0093387s + 0.00076465s^{0.514} \\ + 0.00042503 = 0 \end{aligned} \tag{30}$$

This can be rewritten as

$$\begin{aligned} D(s) = s^{\frac{551.4}{100}} + 0.2985s^{\frac{451.4}{100}} + 4.1151s^{\frac{441.6}{100}} \\ + 0.61855s^{\frac{351.4}{100}} + 1.8961s^{\frac{341.6}{100}} + 0.29863s^{\frac{300}{100}} \\ + 0.24785s^{\frac{251.4}{100}} + 0.12868s^{\frac{241.6}{100}} + 0.1376s^{\frac{200}{100}} \\ + 0.017162s^{\frac{151.4}{100}} + 0.0058568s^{\frac{141.6}{100}} + 0.0093387s^{\frac{100}{100}} \\ + 0.00076465s^{\frac{51.4}{100}} + 0.00042503 = 0 \end{aligned} \tag{31}$$

The following transformation is used to map from s-plane to w-plane.

$$w = s^{\frac{1}{m}}, \quad m = 100 \tag{32}$$

Therefore,

$$\begin{aligned} D(w) = s^{551.4} + 0.2985s^{451.4} + 4.1151s^{441.6} \\ + 0.61855s^{351.4} + 1.8961s^{341.6} + 0.29863s^{300} \\ + 0.24785s^{251.4} + 0.12868s^{241.6} + 0.1376s^{200} \\ + 0.017162s^{151.4} + 0.0058568s^{141.6} + 0.0093387s^{100} \\ + 0.00076465s^{51.4} + 0.00042503 = 0 \end{aligned} \tag{33}$$

The stability conditions for the fractional-order system are given as

- The system is stable if

$$\frac{\pi}{2m} < |arg(w)| < \frac{\pi}{m} \tag{34a}$$

- The system is oscillatory if

$$|arg(w)| = \frac{\pi}{2m} \tag{34b}$$

If not, the system is unstable.

The pole-zero plot is obtained by solving (33) using the fractional-order modeling and control (FOMCON) toolbox, as shown in Figure 22. It shows that the system is stable for $q = 1/m = 0.01$, and all the poles of $s^{0.01}$ polynomial are placed in the stable area (outside the red shaded region), satisfying Matignon's stability theorem [56]. The region of stability depends on the order q. Since, $q = 0.01$, the angle is around 0.9°.

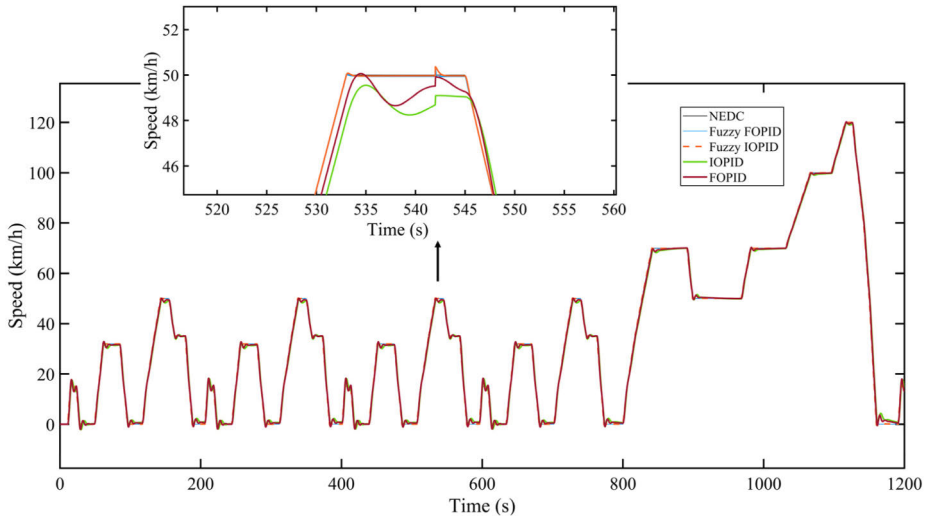

FIGURE 18. Performance of fuzzy FOPID, fuzzy IOPID, FOPID, and IOPID to track NEDC speed test under the influence of disturbance.

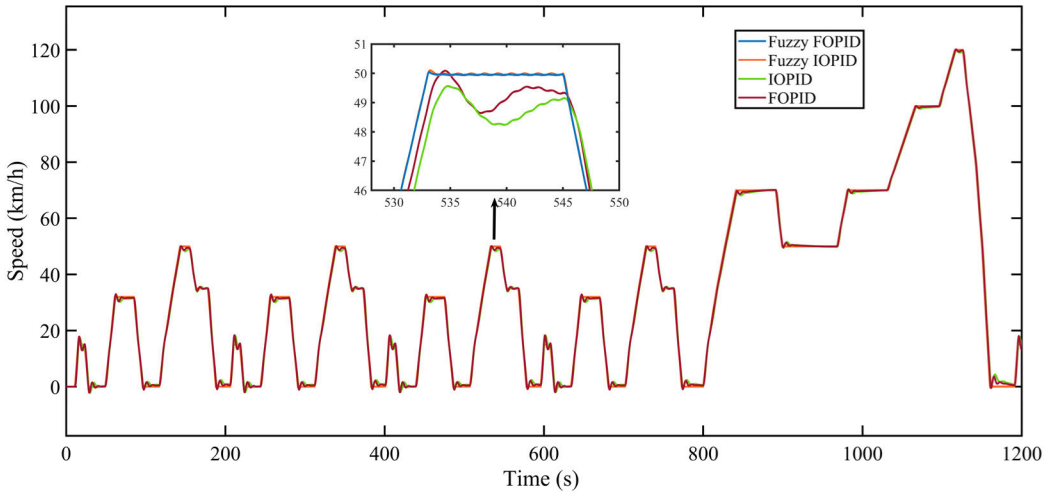

FIGURE 19. Performance of fuzzy FOPID, fuzzy IOPID, FOPID, and IOPID to track NEDC speed test in the presence of measurement noise.

TABLE 7. Comparison of performance of ACO, PSO, and GA based fuzzy FOPID controller for EV speed control.

Controller	Objective function	Settling time (sec)	Rise time (sec)	Overshoot (%)	Steady-state error	ITSE	ITAE	IAE	ISE	Total indices
Fuzzy FOPID ACO	**J_5**	**0.75**	**0.081**	**0.505**	**0.0009**	**0.006**	**5.129**	**0.192**	**0.03**	**5.36**
Fuzzy FOPID GA	J_5	1.4	0.19	0.80	0.0021	0.040	6.12	0.412	0.23	6.80
Fuzzy FOPID PSO	J_5	1.2	0.12	0.72	0.0010	0.020	5.75	0.311	0.11	6.20

Similarly, during ACO, each combination of controller parameters is subjected to stability check using the Matignon stability theorem. Hence, all the controller parameter values that cause instability of the closed-loop system are rejected.

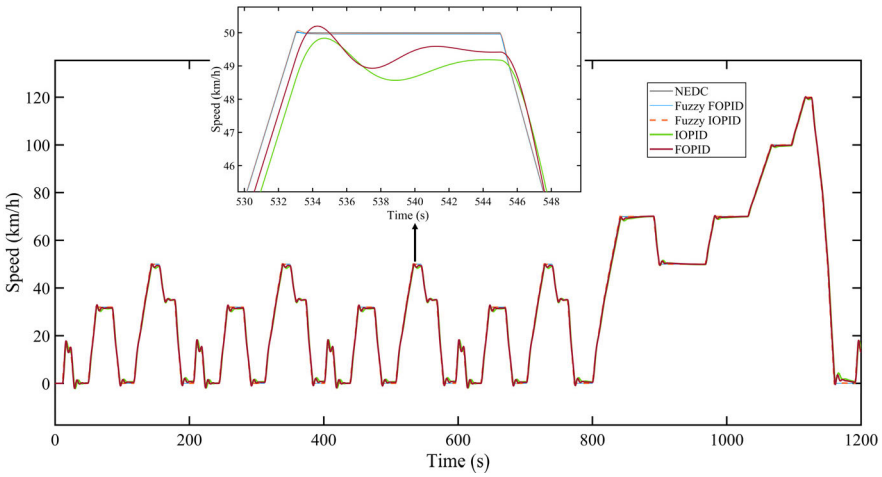

FIGURE 20. Robustness of fuzzy FOPID, fuzzy IOPID, FOPID, and IOPID against the parameter variations of EV, i.e., change in mass by +30%, rolling resistance coefficient by +30%, drag coefficient by −20%, and EV tire radius by +25%.

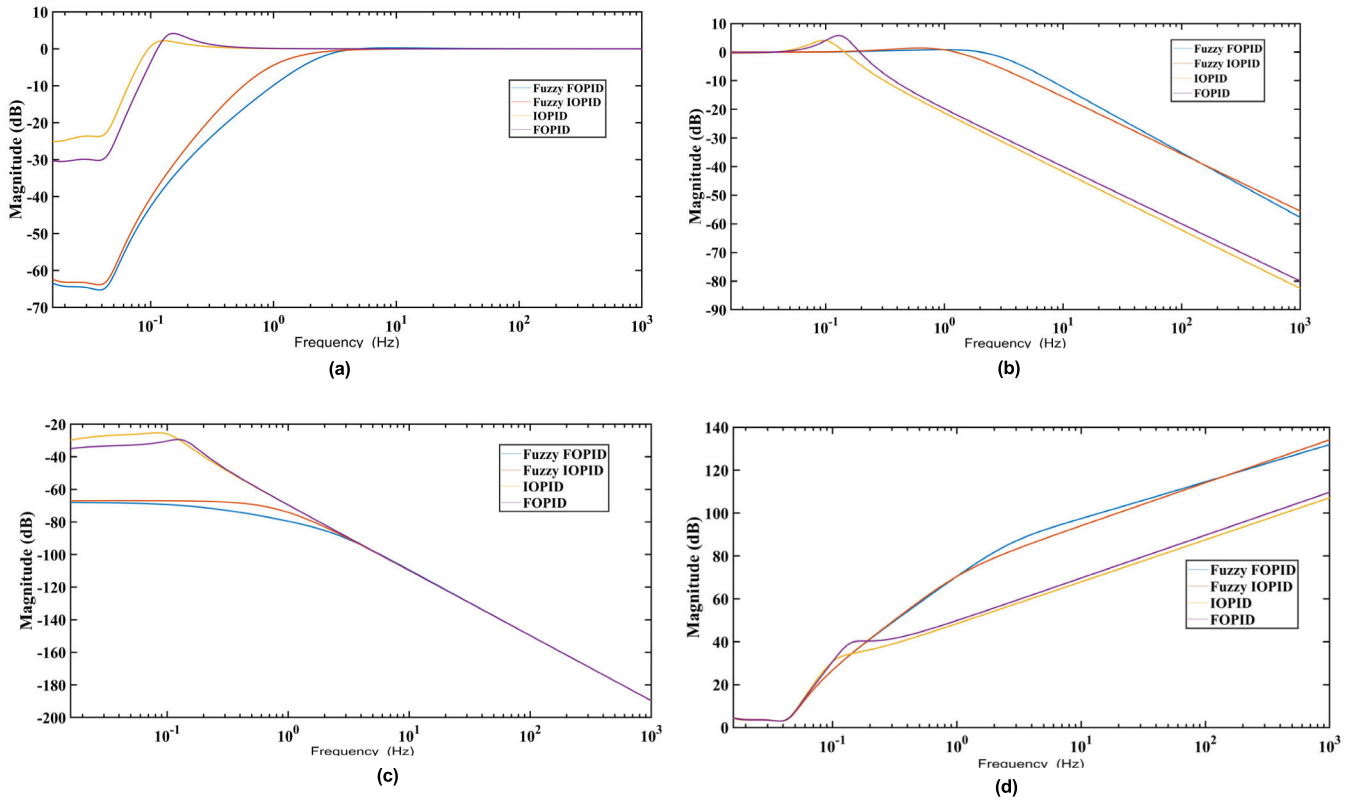

FIGURE 21. Frequency domain plots of (a) Sensitivity function, (b) Complementary sensitivity function, (c) Disturbance sensitivity, and (d) Control sensitivity using fuzzy FOPID, fuzzy IOPID, FOPID, and IOPID controllers.

f. Eigenvalue Analysis: The eigenvalues of the compensated system can be determined using the characteristic equation given by

$$|\lambda I - A_c| = 0 \tag{35}$$

where A_c is the system matrix of the linearized system with the selected controller, λ is the eigenvalues, and I is the identity matrix.

Theorem: If all the eigenvalues of A_c satisfy the condition

$$|arg(\lambda(A_c))| > \frac{q\pi}{2} \tag{36}$$

then the zero solution of the system is asymptotically stable. The proof of this theorem is detailed in [56].

There are 551 roots, and all roots of the characteristic equation satisfy the (36) and lie within the stable region,

TABLE 8. Comparison of performance of ACO based fuzzy controller with other existing controllers.

Criteria	ACO Fuzzy FOPID [This work]	PI [44]	Fuzzy PI [44]	MPC [4]
SSE	**2.711**	14.021	10.600	7.090
MAE	**0.005**	0.101	0.0984	0.010
MSE	**6.100 x 10^{-5}**	9.919 x 10^{-4}	4.697 x 10^{-4}	1.990 x 10^{-4}

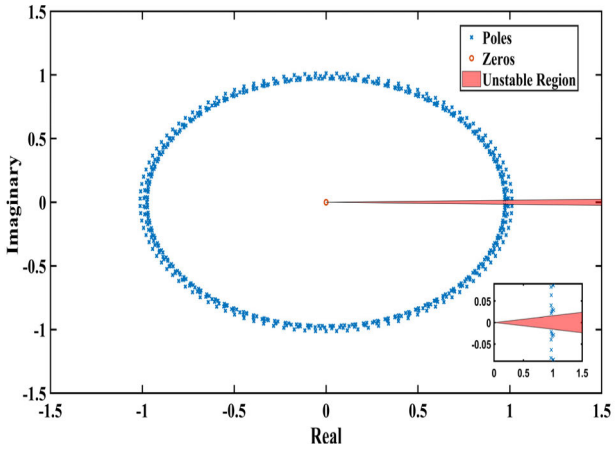

FIGURE 22. Stability plot for the closed-loop EV system.

TABLE 9. Design details for three input EX-CCII and three input summation circuits.

Process	180 nm GPDK CMOS	
Supply voltage	$V_{DD} = -V_{SS}$	0.9 V
Three input EX-CCII circuit in Fig. 10 (a)	I_0	12 µA
	$\left(\frac{W}{L}\right)_{Mn1-Mn4}$	$\frac{25\ \mu m}{2\ \mu m}$
	$\left(\frac{W}{L}\right)_{Mn5-Mn10}$	$\frac{1\ \mu m}{5\ \mu m}$
	I_B	10 µA
	R	5.8 kΩ
Three input summation circuit in Fig. 10 (b)	$\left(\frac{W}{L}\right)_{Mn1a-Mn6a}$	$\frac{20\ \mu m}{2\ \mu m}$
	$\left(\frac{W}{L}\right)_{Mp1a-Mp2a}$	$\frac{25\ \mu m}{1\ \mu m}$

as shown in Figure 22. This condition assures that the system is bounded input bounded output (BIBO) stable and asymptotically stable.

g. Comparison of ACO Based Fuzzy FOPID Controller With Other Optimization Algorithms and Existing Controllers:

The ACO-based fuzzy FOPID controller's speed tracking performance is compared with the GA-based fuzzy FOPID controller and the PSO-based fuzzy FOPID controller. The parameters considered for the PSO are the maximum iteration = 100, population size = 100, acceleration factors $c_1 = c_2 = 2$ and inertia weights $wmax = 0.9$ and $wmin = 0.4$. Similarly, the parameters of the GA optimization are also selected. Here, maximum generation is taken as 100, population size = 100, crossover fraction = 0.8 and mutation fraction = 0.2. In all the cases, J_5 is considered as the objective function to be minimized. Here, the lower and upper bounds of the controller parameters and adjustable membership parameters are taken from Table 3. Table 7 gives the EV time-domain performance and the performance indices using the above-considered controllers. It is evident from the results that the ACO-based fuzzy FOPID controller is better than the other controllers. Also, the PSO-based fuzzy FOPID controller gives better performance than the GA-based controller.

Three standard error measurement criteria that can evaluate the efficiency of the proposed controller with other existing controllers are the sum of squared errors (SSE), mean absolute error (MAE), and mean square error (MSE). Table 8 shows the performance comparison of the proposed controller to multi-objective PI [30], multi-objective fuzzy PI [30], and model predictive control (MPC) [4] controllers. It is observed that the proposed controller yields an optimal performance as the values of their error measurement criteria are close to zero.

Despite the various merits of the schemes discussed, it has a couple of limitations: (i) Framing the fuzzy rule base for the fuzzy logic controller to track the new European

TABLE 10. Values of resistors, DC bias currents, and capacitors of Valsa RC networks used to realize fractional-order capacitors.

Element	C_λ=10 µ/sec$^{0.486}$	C_μ = 10 µ/sec$^{0.0908}$
R_p (I_p)	374.74 kΩ (210 nA)	4.27 MΩ (16 nA)
R_1 (I_1)	189.86 kΩ (450 nA)	740.4 kΩ (100 nA)
R_2 (I_2)	63.84 kΩ (1.5 µA)	109.3 kΩ (830 nA)
R_3 (I_3)	21.47 kΩ (5 µA)	16.15 kΩ (7 µA)
R_4 (I_4)	7.22 kΩ (19 µA)	2.38 kΩ (160 µA)
R_5 (I_5)	2.42 kΩ (100 µA)	1 kΩ (330 µA)
C_p	75.41 µF	4.05 µF
C_1	8.38 µF	2.15 µF
C_2	2.99 µF	1.74 µF
C_3	1.06 µF	1.41 µF
C_4	380.90 nF	1.15 µF
C_5	135.92 nF	936 nF

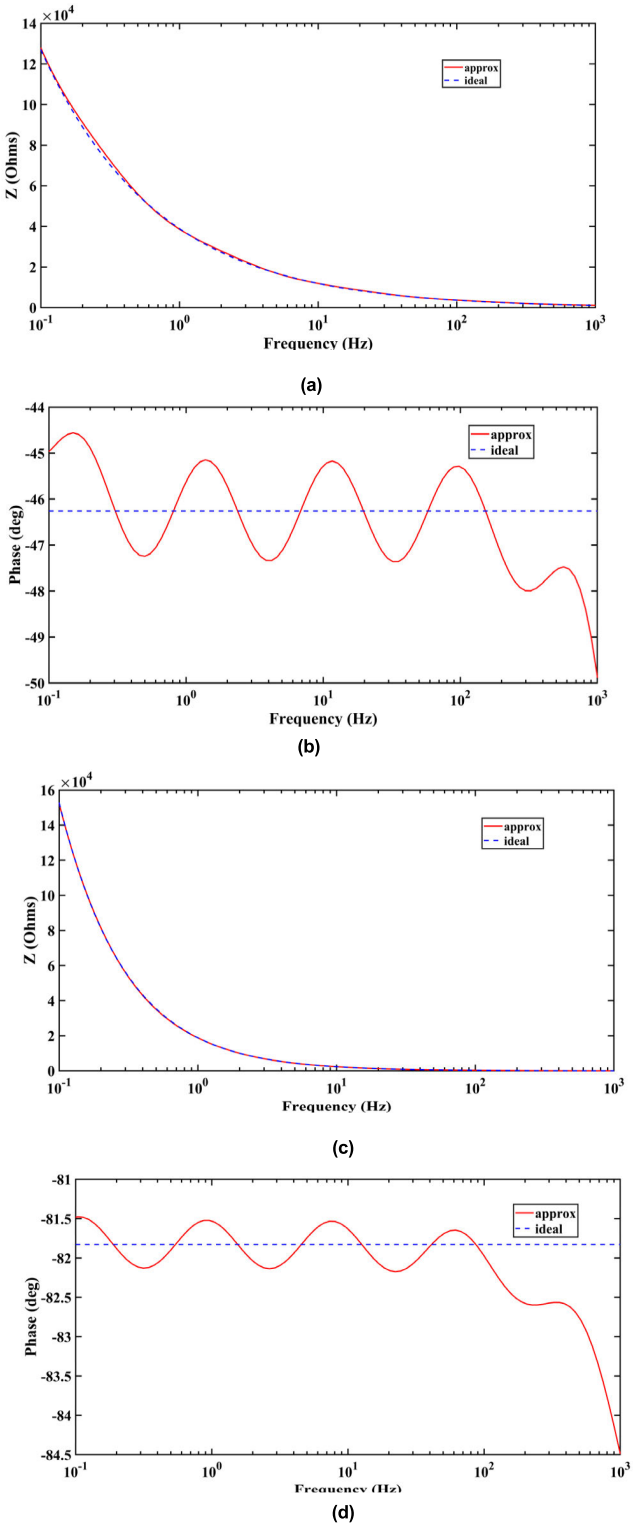

FIGURE 23. Impedance frequency response of Valsa RC networks approximating the fractional-order capacitors: $C_\lambda = 10\ \mu/\text{sec}^{0.486}$ (a) magnitude (b) phase and $C_\mu = 10\ \mu/\text{sec}^{0.0908}$ (c) magnitude, (d) phase.

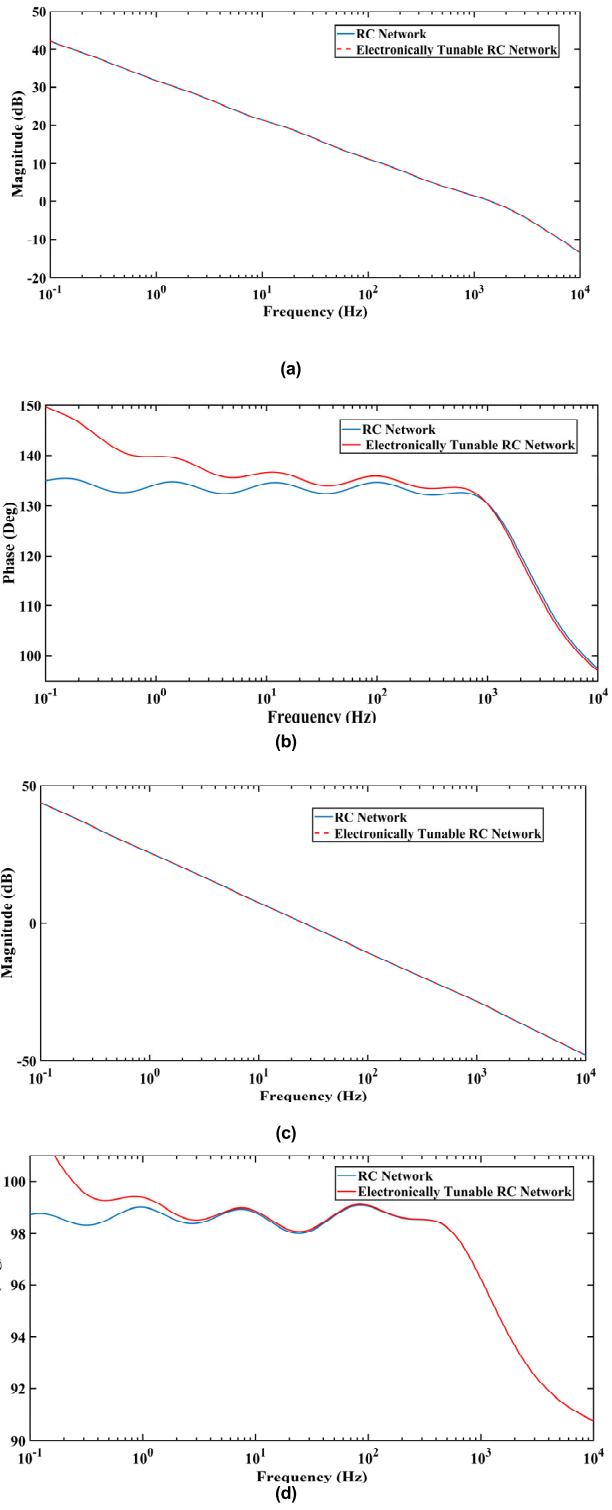

FIGURE 24. Frequency response of Valsa RC networks using passive resistors and electronically tunable resistors used to realize the fractional-order capacitors: $C_\lambda = 10\ \mu/\text{sec}^{0.486}$ (a) magnitude, (b) phase and $C_\mu = 10\ \mu/\text{sec}^{0.0908}$ (c) magnitude, (d) phase.

drive cycle (NEDC) test is time-consuming as it requires expertise and experience. (ii) More number of parameters (eight parameters) are used in optimization.

A. CIRCUIT REALIZATION OF FOPID CONTROLLER

The EX-CCII based FOPID controller circuit in Figure 8 is simulated in the Cadence analog design environment using

TABLE 11. Comparison of the proposed controller scheme with other existing solutions.

Factors	This work	[32]	[33]	[57]	[35]	[34]
Technology	**CMOS (GPDK 180 nm)**	CMOS (AMS 0.35 µm)	CMOS (AMS 0.35 µm)	----	CMOS ON (0.7 µm)	CMOS (AMS 0.35 µm)
No. of active blocks	**1 EX-CCII +14 OTAs**	29 OTAs	16 OTAs	20 CFOAs	4 VDCCs	1 EX-CCII
No. of resistors and capacitors	**12C**	10C	6C	44R +10C	10R+8C	14R+12C
All grounded capacitors	**Yes**	Yes	Yes	Yes	Yes	Yes
Electronic tuning	**Yes**	Yes	Yes	No	Yes	No

R - Resistor, C - Capacitor, OTA - Operational transconductance amplifier, EX-CCII - Extra input CCII, CFOA - Current feedback operational amplifier, VDCC – Voltage differencing current conveyor

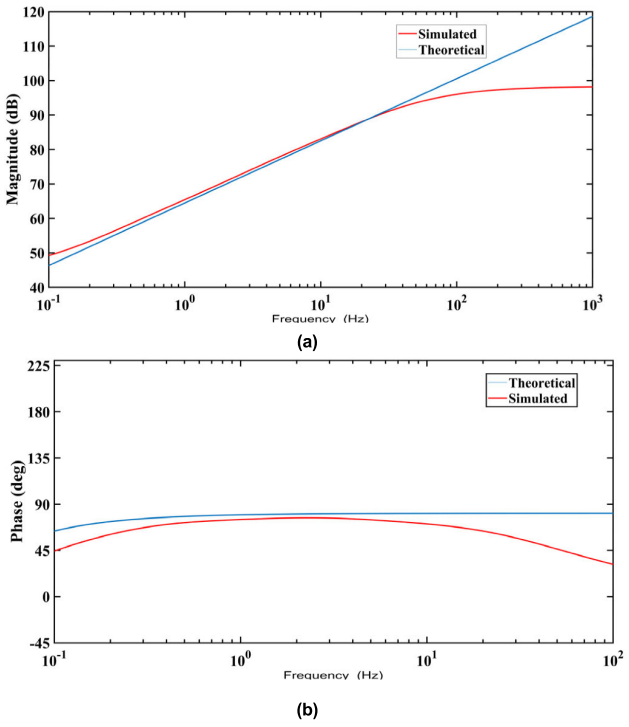

FIGURE 25. Frequency response of the designed controller (a) magnitude, (b) phase.

a 180 nm GPDK CMOS process. Table 9 shows the design details and aspect ratios (W/L) for MOS transistors used in Figure 10.

In the CMOS circuit of three input EX-CCII, all transistors operate in the saturation region, and DC bias current I_0 is distributed using the NMOS and the PMOS current mirrors with the aspect ratios 5 μm/1μm and 25 μm/5μm, respectively.

Similarly, the DC bias current I_B in the summation stage is distributed using the NMOS and PMOS current mirrors with aspect ratios 2.5 μm/1 μm and 24 μm/10 μm, respectively.

The fuzzy FOPID controller parameters in (29) are used to evaluate the performance of the FOPID controller circuit in Figure 8. Using Eq. (22) and (29), the circuit parameters are calculated as $R_1 = 1$ kΩ, $R_2 = 39.12$ kΩ, $R_\lambda = 4.319$ kΩ, $C_\lambda = 10\ \mu/\text{sec}^{0.486}$, $R_\mu = 31.19$ MΩ and $C_\mu = 10\ \mu/\text{sec}^{0.0908}$.

The fractional-order capacitors used in the fractional-order differentiator and the integrator stages are approximated using the 5$^{\text{th}}$ order modified Oustaloup method and realized using the Valsa RC networks, given in Figure 9, to cover the frequency range [0.1 Hz, 1000 Hz] with the phase accuracy of 1°. The behaviour of the Valsa RC network used to implement the constant phase element is verified by plotting the impedance frequency response, along with the ideal response, as shown in Figure 23. The resistors in a Valsa RC network are realized using the CMOS circuits of electronically tunable OTA simulated resistors in Figure 12, and their values are tuned by adjusting the bias current.

Here, the $R = 1/g_m$, where g_m is the transconductance of the differential MOS pair in Figure 12, and the values of DC bias currents are calculated using (25a)-(25b). Also, the aspect ratios of the MOS transistors Mp1b-Mp4b are set as 25 μm/2 μm and Mn1b-Mn4b as 10 μm/ 2μm. Table 10 summarizes the value of resistors, dc bias currents, and capacitors used in the Valsa RC network.

Figure 24 presents the magnitude and phase responses of the Valsa RC networks using the passive resistors and the electronically tunable resistors. It shows that the magnitude response error is negligible, and the error in the phase plot is about 10%. These errors are caused due to the OTA's imperfections. The gain and phase responses of EX-CCII based FOPID controller circuits are depicted in Figure 25, which confirm the controller's accurate operation. Any set of the controller parameters of the fuzzy FOPID controller can be realized using the circuit, shown in Figure 8, by electronically tuning the OTA simulated resistors.

Table 11 shows the comparison of the critical features of the proposed FOPID circuit to other previously reported solutions based on various active elements. Based on Table 11, it is evident that in the proposed scheme, there is a significant reduction in active element count and passive resistors. OTA-based simulated resistors replace the passive resistors in the controller circuit and offer electronic tunability.

VI. CONCLUSION

This study presents a novel approach in designing and developing a multi-objective fuzzy FOPID for speed control of EV. The EV can be controlled in real-time by adjusting the control

parameters and the membership functions via ACO when the system encounters disturbance, parameter uncertainties, and varying road conditions. The fuzzy fractional-order controllers have become industrial control standards due to their improved robustness against plant parameter variations and system perturbation, and better disturbance rejection control. The controller's significant advantage is its ability to reduce control effort, reducing the energy wasted in various industrial control applications.

The proposed controller can be effectively employed for EV speed tracking. The effectiveness and the robustness of the proposed novel controller have been comprehensively illustrated by subjecting it to disturbance and uncertainties.

The significant outcomes of this investigation are summarized as:

1. The performance of ACO-based fuzzy FOPID was compared with the fuzzy IOPID, FOPID, and classical IOPID, and it was observed that the proposed controller gave the fastest tracking response with a settling time of 0.75 sec and a rise time of 0.081 sec. The controller exhibited a small overshoot of 0.5% and a steady-state error of 0.0001. Furthermore, the proposed controller gives a remarkable reduction in error indices, such as *IAE*, *ISE*, *ITAE*, and *ITSE*, by 87%, 93%, 78%, and 98%, respectively, when compared with other controllers.
2. The simulation results also revealed that the proposed controller could excellently handle parameter variation, uncertainties, disturbance, and noise compared to the other controllers. The proposed controller's robustness was tested under the following EV parameter variations from its nominal value, i.e., change in mass +30%, change in rolling resistance +30%, change in drag coefficient -20%, and change in EV tire radius +25%.
3. The stability of the system is also investigated using Matignon's stability theorem and eigenvalue analysis.
4. The ACO-based fuzzy FOPID controller's speed tracking performance was evaluated and compared with the PSO and the GA optimized fuzzy FOPID controllers. It was found that the ACO-based controller gave a faster convergence and low values of performance indices, i.e., $ITSE = 0.006$, $ITAE = 5.129$, $IAE = 0.192$, $ISE = 0.03$, and the sum of indices was 5.36.
5. The proposed controller was realized using a single EX-CCII block that offered design flexibility and electronic tunability. It also allowed the simultaneous realization of the fractional-order integrator and differentiator stages of different orders. This circuit can be used to realize any combination of the fuzzy FOPID controller parameters by adjusting the bias currents in OTA-based resistors. The proposed circuit uses a minimum number of passive elements that make it energy effective. The controller can be implemented using the integrated circuits of analog blocks, and its performance can be verified in real-time.

This investigation expects to give valuable insights for future simulation studies that can be validated using the real-time experimental setup to control EVs' speed. The proposed fuzzy FOPID controller is well suited for cruise control applications in EV and can also be used in EV battery recharging or discharging applications under constant DC voltage. As a future scope, the fuzzy-based controller can be extended to an Adaptive Neuro-Fuzzy Inference System (ANFIS), which combines the advantages of fuzzy inference systems and neural networks. It provides better learning and adaptation capability without requiring expert knowledge.

REFERENCES

[1] M. Veysi, J. Aghaei, M. Shasadeghi, R. Razzaghi, B. Bahrani, and D. J. Ryan, "Energy-efficient speed control of electric vehicles: Linear matrix inequality approach," *IEEE Trans. Veh. Technol.*, vol. 69, no. 10, pp. 10469–10483, Oct. 2020, doi: 10.1109/tvt.2020.3008500.

[2] M. S. Kumar and S. T. Revankar, "Development scheme and key technology of an electric vehicle: An overview," *Renew. Sustain. Energy Rev.*, vol. 70, pp. 1266–1285, Apr. 2017, doi: 10.1016/j.rser.2016.12.027.

[3] W.-J. Lee, G. Strbac, Z. Hu, Z. Ding, P. Sarikprueck, F. Teng, and G. Kariniotakis, "Special issue on advanced approaches and applications for electric vehicle charging demand management," *IEEE Trans. Ind. Appl.*, vol. 56, no. 5, pp. 5682–5683, Sep. 2020, doi: 10.1109/tia.2020.3003567.

[4] M. H. Khooban, N. Vafamand, and T. Niknam, "T–S fuzzy model predictive speed control of electrical vehicles," *ISA Trans.*, vol. 64, pp. 231–240, Sep. 2016, doi: 10.1016/j.isatra.2016.04.019.

[5] M. H. Khooban, T. Niknam, F. Blaabjerg, and M. Dehghani, "Free chattering hybrid sliding mode control for a class of non-linear systems: Electric vehicles as a case study," *IET Sci., Meas. Technol.*, vol. 10, no. 7, pp. 776–785, Oct. 2016, doi: 10.1049/iet-smt.2016.0091.

[6] K. J. Åström and T. Hägglund, "The future of PID control," *Control Eng. Pract.*, vol. 9, no. 11, pp. 1163–1175, Apr. 2001, doi: 10.1016/S0967-0661(01)00062-4.

[7] K. Heong Ang, G. Chong, and Y. Li, "PID control system analysis, design, and technology," *IEEE Trans. Control Syst. Technol.*, vol. 13, no. 4, pp. 559–576, Jul. 2005, doi: 10.1109/TCST.2005.847331.

[8] Y. Arya, "Impact of ultra-capacitor on automatic generation control of electric energy systems using an optimal FFOID controller," *Int. J. Energy Res.*, pp. 8765–8778, Aug. 2019, doi: 10.1002/er.4767.

[9] K. Premkumar and B. V. Manikandan, "Bat algorithm optimized fuzzy PD based speed controller for brushless direct current motor," *Eng. Sci. Technol., Int. J.*, vol. 19, no. 2, pp. 818–840, Jun. 2016, doi: 10.1016/j.jestch.2015.11.004.

[10] M. Rabah, A. Rohan, Y.-J. Han, and S.-H. Kim, "Design of fuzzy-PID controller for quadcopter trajectory-tracking," *Int. J. FUZZY Log. Intell. Syst.*, vol. 18, no. 3, pp. 204–213, Sep. 2018, doi: 10.5391/IJFIS.2018.18.3.204.

[11] B. E. Demir, R. Bayir, and F. Duran, "Real-time trajectory tracking of an unmanned aerial vehicle using a self-tuning fuzzy proportional integral derivative controller," *Int. J. Micro Air Vehicles*, vol. 8, no. 4, pp. 252–268, Dec. 2016, doi: 10.1177/1756829316675882.

[12] Y. Tao, J. Zheng, Y. Lin, T. Wang, H. Xiong, G. He, and D. Xu, "Fuzzy PID control method of deburring industrial robots," *J. Intell. Fuzzy Syst.*, vol. 29, no. 6, pp. 2447–2455, Oct. 2015, doi: 10.3233/IFS-151945.

[13] Y. Arya, "AGC performance enrichment of multi-source hydrothermal gas power systems using new optimized FOFPID controller and redox flow batteries," *Energy*, vol. 127, pp. 704–715, May 2017, doi: 10.1016/j.energy.2017.03.129.

[14] P. Khatun, C. M. Bingham, N. Schofield, and P. H. Mellor, "Application of fuzzy control algorithms for electric vehicle antilock braking/traction control systems," *IEEE Trans. Veh. Technol.*, vol. 52, no. 5, pp. 1356–1364, Sep. 2003, doi: 10.1109/TVT.2003.815922.

[15] S. Poiurani, K. U. Kumar, and S. Renganarayanan, "Intelligent controller design for electric vehicle," in *Proc. 57th IEEE Semiannual Veh. Technol. Conf. (VTC-Spring)*, vol. 4, Apr. 2003, pp. 2447–2450, doi: 10.1109/vetecs.2003.1208830.

[16] C. A. Monje, B. M. Vinagre, V. Feliu, and Y. Chen, "Tuning and auto-tuning of fractional order controllers for industry applications," *Control Eng. Pract.*, vol. 16, no. 7, pp. 798–812, Jul. 2008, doi: 10.1016/j.conengprac.2007.08.006.

[17] F. Padula and A. Visioli, "Tuning rules for optimal PID and fractional-order PID controllers," *J. Process Control*, vol. 21, no. 1, pp. 69–81, Jan. 2011, doi: 10.1016/j.jprocont.2010.10.006.

[18] A. Tepljakov, E. A. Gonzalez, E. Petlenkov, J. Belikov, C. A. Monje, and I. Petráš, "Incorporation of fractional-order dynamics into an existing PI/PID DC motor control loop," *ISA Trans.*, vol. 60, pp. 262–273, Jan. 2016, doi: 10.1016/j.isatra.2015.11.012.

[19] D. Guha, P. K. Roy, S. Banerjee, S. Padmanaban, F. Blaabjerg, and D. Chittathuru, "Small-signal stability analysis of hybrid power system with quasi-oppositional sine cosine algorithm optimized fractional order PID controller," *IEEE Access*, vol. 8, pp. 155971–155986, 2020, doi: 10.1109/ACCESS.2020.3018620.

[20] H. K, Abdulkhader, J. Jacob, and A. T. Mathew, "Robust type-2 fuzzy fractional order PID controller for dynamic stability enhancement of power system having RES based microgrid penetration," *Int. J. Electr. Power Energy Syst.*, vol. 110, pp. 357–371, Sep. 2019, doi: 10.1016/j.ijepes.2019.03.027.

[21] M. A. Hannan, J. A. Ali, M. S. H. Lipu, A. Mohamed, P. J. Ker, T. M. I. Mahlia, M. Mansor, A. Hussain, K. M. Muttaqi, and Z. Y. Dong, "Role of optimization algorithms based fuzzy controller in achieving induction motor performance enhancement," *Nature Commun.*, vol. 11, no. 1, pp. 1–11, Jul. 2020, doi: 10.1038/s41467-020-17623-5.

[22] S. Çeven, A. Albayrak, and R. Bayır, "Real-time range estimation in electric vehicles using fuzzy logic classifier," *Comput. Electr. Eng.*, vol. 83, May 2020, Art. no. 106577, doi: 10.1016/j.compeleceng.2020.106577.

[23] A. Rubaai, M. J. Castro-Sitiriche, and A. R. Ofoli, "DSP-based laboratory implementation of hybrid fuzzy-PID controller using genetic optimization for high-performance motor drives," *IEEE Trans. Ind. Appl.*, vol. 44, no. 6, pp. 1977–1986, Nov. 2008, doi: 10.1109/TIA.2008.2006347.

[24] I. Pan, S. Das, and A. Gupta, "Tuning of an optimal fuzzy PID controller with stochastic algorithms for networked control systems with random time delay," *ISA Trans.*, vol. 50, no. 1, pp. 28–36, Jan. 2011, doi: 10.1016/j.isatra.2010.10.005.

[25] J. A. Ali, M. A. Hannan, A. Mohamed, and M. G. M. Abdolrasol, "Fuzzy logic speed controller optimization approach for induction motor drive using backtracking search algorithm," *Measurement*, vol. 78, pp. 49–62, Jan. 2016, doi: 10.1016/j.measurement.2015.09.038.

[26] O. Castillo, F. Valdez, J. Soria, L. Amador-Angulo, P. Ochoa, and C. Peraza, "Comparative study in fuzzy controller optimization using bee colony, differential evolution, and harmony search algorithms," *Algorithms*, vol. 12, no. 1, pp. 1–21, Jan. 2019, doi: 10.3390/a12010009.

[27] S. Das, I. Pan, S. Das, and A. Gupta, "A novel fractional order fuzzy PID controller and its optimal time domain tuning based on integral performance indices," *Eng. Appl. Artif. Intell.*, vol. 25, no. 2, pp. 430–442, Mar. 2012, doi: 10.1016/j.engappai.2011.10.004.

[28] V. Kumar, K. P. S. Rana, and P. Mishra, "Robust speed control of hybrid electric vehicle using fractional order fuzzy PD and PI controllers in cascade control loop," *J. Franklin Inst.*, vol. 353, no. 8, pp. 1713–1741, May 2016, doi: 10.1016/j.jfranklin.2016.02.018.

[29] A. Zamani, S. M. Barakati, and S. Yousofi-Darmian, "Design of a fractional order PID controller using GBMO algorithm for load–frequency control with governor saturation consideration," *ISA Trans.*, vol. 64, pp. 56–66, Sep. 2016, doi: 10.1016/j.isatra.2016.04.021.

[30] M. Al-Dhaifallah, N. Kanagaraj, and K. S. Nisar, "Fuzzy fractional-order PID controller for fractional model of pneumatic pressure system," *Math. Probl. Eng.*, vol. 2018, Jan. 2018, Art. no. 5478781, doi: 10.1155/2018/5478781.

[31] X. Wu, Y. Xu, J. Liu, C. Lv, J. Zhou, and Q. Zhang, "Characteristics analysis and fuzzy fractional-order PID parameter optimization for primary frequency modulation of a pumped storage unit based on a multi-objective gravitational search algorithm," *Energies*, vol. 13, no. 1, p. 137, Dec. 2019, doi: 10.3390/en13010137.

[32] I. Dimeas, I. Petras, and C. Psychalinos, "New analog implementation technique for fractional-order controller: A DC motor control," *AEU-Int. J. Electron. Commun.*, vol. 78, pp. 192–200, Aug. 2017, doi: 10.1016/j.aeue.2017.03.010.

[33] S. Kapoulea, V. Bizonis, P. Bertsias, C. Psychalinos, A. Elwakil, and I. Petráš, "Reduced active components count electronically adjustable fractional-order controllers: Two design examples," *Electronics*, vol. 9, no. 1, p. 63, Jan. 2020, doi: 10.3390/electronics9010063.

[34] S. Kapoulea, C. Psychalinos, and A. S. Elwakil, "Single active element implementation of fractional-order differentiators and integrators," *AEU-Int. J. Electron. Commun.*, vol. 97, pp. 6–15, Dec. 2018, doi: 10.1016/j.aeue.2018.09.046.

[35] O. Domansky, R. Sotner, L. Langhammer, J. Jerabek, C. Psychalinos, and G. Tsirimokou, "Practical design of RC approximants of constant phase elements and their implementation in fractional-order PID regulators using CMOS voltage differencing current conveyors," *Circuits, Syst., Signal Process.*, vol. 38, no. 4, pp. 1520–1546, Apr. 2019, doi: 10.1007/s00034-018-0944-z.

[36] R. Sharma, K. P. S. Rana, and V. Kumar, "Performance analysis of fractional order fuzzy PID controllers applied to a robotic manipulator," *Expert Syst. Appl.*, vol. 41, no. 9, pp. 4274–4289, Jul. 2014, doi: 10.1016/j.eswa.2013.12.030.

[37] C.-S. Shieh, "Fuzzy PWM based on genetic algorithm for battery charging," *Appl. Soft Comput.*, vol. 21, pp. 607–616, Aug. 2014, doi: 10.1016/j.asoc.2014.04.009.

[38] A. Mughees and S. A. Mohsin, "Design and control of magnetic levitation system by optimizing fractional order PID controller using ant colony optimization algorithm," *IEEE Access*, vol. 8, pp. 116704–116723, 2020, doi: 10.1109/ACCESS.2020.3004025.

[39] M. Birattari, P. Pellegrini, and M. Dorigo, "On the invariance of ant colony optimization," *IEEE Trans. Evol. Comput.*, vol. 11, no. 6, pp. 732–742, Dec. 2007, doi: 10.1109/TEVC.2007.892762.

[40] M. Wang, T. Ma, G. Li, X. Zhai, and S. Qiao, "Ant colony optimization with an improved pheromone model for solving MTSP with capacity and time window constraint," *IEEE Access*, vol. 8, pp. 106872–106879, 2020, doi: 10.1109/access.2020.3000501.

[41] J. Yu, R. Li, Z. Feng, A. Zhao, Z. Yu, Z. Ye, and J. Wang, "A novel parallel ant colony optimization algorithm for warehouse path planning," *J. Control Sci. Eng.*, vol. 2020, Aug. 2020, Art. no. 5287189, doi: 10.1155/2020/5287189.

[42] M. S. Semary, M. E. Fouda, H. N. Hassan, and A. G. Radwan, "Realization of fractional-order capacitor based on passive symmetric network," *J. Adv. Res.*, vol. 18, pp. 147–159, Jul. 2019, doi: 10.1016/j.jare.2019.02.004.

[43] G. Tsirimokou, C. Psychalinos, and A. S. Elwakil, "Emulation of a constant phase element using operational transconductance amplifiers," *Anal. Integr. Circuits Signal Process.*, vol. 85, no. 3, pp. 413–423, Dec. 2015, doi: 10.1007/s10470-015-0626-8.

[44] M. H. Khooban, M. Shasadeghi, T. Niknam, and F. Blaabjerg, "Analysis, control and design of speed control of electric vehicles delayed model: Multi-objective fuzzy fractional-order $PI^{\lambda}D^{\mu}$ controller," *IET Sci., Meas. Technol.*, vol. 11, no. 3, pp. 249–261, May 2017, doi: 10.1049/iet-smt.2016.0277.

[45] V. Sharma and S. Purwar, "Nonlinear controllers for a light-weighted all-electric vehicle using Chebyshev neural network," *Int. J. Veh. Technol.*, vol. 2014, Apr. 2014, Art. no. 867209, doi: 10.1155/2014/867209.

[46] P. Shah and S. Agashe, "Review of fractional PID controller," *Mechatronics*, vol. 38, pp. 29–41, Sep. 2016, doi: 10.1016/j.mechatronics.2016.06.005.

[47] I. Pan and S. Das, "Kriging based surrogate modeling for fractional order control of microgrids," *IEEE Trans. Smart Grid*, vol. 6, no. 1, pp. 36–44, Jan. 2015, doi: 10.1109/TSG.2014.2336771.

[48] M. S. Mahmoud, *Fuzzy Control, Estimation and Diagnosis: Single and Interconnected Systems*. Riyadh, Saudi Arabia: Springer, 2018.

[49] H. Bin Duan, D. Bo Wang, and X. Fen Yu, "Novel approach to nonlinear PID parameter optimization using ant colony optimization algorithm," *J. Bionic Eng.*, vol. 3, no. 2, pp. 73–78, Jun. 2006, doi: 10.1016/S1672-6529(06)60010-3.

[50] S. Das, I. Pan, and S. Das, "Performance comparison of optimal fractional order hybrid fuzzy PID controllers for handling oscillatory fractional order processes with dead time," *ISA Trans.*, vol. 52, no. 4, pp. 550–566, Jul. 2013, doi: 10.1016/j.isatra.2013.03.004.

[51] S. Kapoulea, C. Psychalinos, and A. S. Elwakil, "Realizations of simple fractional-order capacitor emulators with electronically-tunable capacitance," *Integration*, vol. 69, pp. 225–233, Nov. 2019, doi: 10.1016/j.vlsi.2019.04.004.

[52] S. A. Tekin and M. Alçı, "Design and applications of electronically tunable floating resistor using differential amplifier," *Electron. Electr. Eng.*, vol. 19, no. 4, pp. 41–46, Apr. 2013, doi: 10.5755/j01.eee.19.4.1310.

[53] Q. Huang, Z. Huang, and H. Zhou, "Nonlinear optimal and robust speed control for a light-weighted all-electric vehicle," *IET Control Theory Appl.*, vol. 3, no. 4, pp. 437–444, Apr. 2009, doi: 10.1049/iet-cta.2007.0367.

[54] P. Anantachaisilp and Z. Lin, "Fractional order PID control of rotor suspension by active magnetic bearings," *Actuators*, vol. 6, no. 1, pp. 1–31, Jan. 2017, doi: 10.3390/act6010004.

[55] A. X. R. Irudayaraj, N. I. A. Wahab, M. G. Umamaheswari, M. A. M. Radzi, N. B. Sulaiman, V. Veerasamy, S. C. Prasanna, and R. Ramachandran, "A Matignon's theorem based stability analysis of hybrid power system for automatic load frequency control using atom search optimized FOPID controller," *IEEE Access*, vol. 8, pp. 168751–168772, 2020, doi: 10.1109/ACCESS.2020.3021212.
[56] D. Qian, C. Li, R. P. Agarwal, and P. J. Y. Wong, "Stability analysis of fractional differential system with Riemann–Liouville derivative," *Math. Comput. Model.*, vol. 52, nos. 5–6, pp. 862–874, Sep. 2010, doi: 10.1016/j.mcm.2010.05.016.
[57] G. Tsirimokou, A. Kartci, J. Koton, N. Herencsar, and C. Psychalinos, "Comparative study of discrete component realizations of fractional-order capacitor and inductor active emulators," *J. Circuits, Syst. Comput.*, vol. 27, no. 11, Oct. 2018, Art. no. 1850170, doi: 10.1142/S0218126618501700.

MARY ANN GEORGE (Graduate Student Member, IEEE) was born in India, in 1991. She received the bachelor's degree in electronics and communication engineering (ECE) and the master's degree in digital electronics and advanced communication from the Manipal Institute of Technology (MIT), Manipal Academy of Higher Education (MAHE), India, in 2013 and 2016, respectively. She is currently pursuing the Ph.D. degree with the ECE Department, MIT, Manipal.

Her research interests include fractional-order controllers, fractional-order systems, and analog circuits. She is a Life Member of the Indian Society of Systems for Science and Engineering (ISSE).

DATTAGURU V. KAMAT (Senior Member, IEEE) was born in India, in 1965. He received the B.E. degree in electronics and communication and the M.E. degree in digital electronics from the B.V. Bhoomaraddi College of Engineering, Karnataka University, Dharwad, in 1987 and 1997, respectively, and the Ph.D. degree in analogue VLSI signal processing from the Manipal Academy of Higher Education (MAHE), Manipal, India, in 2013.

He is currently working as a Professor with the Department of Electronics and Communication Engineering, Manipal Institute of Technology, Manipal. His research contribution includes one U.S. patent granted at WIPO, more than 20 full regular articles published in indexed international journals, and 20 indexed international conference publications. His research interests include digital, analog, and mixed-signal VLSI design, analog VLSI signal processing, digital VLSI architectures, and fractional-order circuits.

Dr. Kamat is a member of IET, IE (India), and ISTE (India).

CIJI PEARL KURIAN (Senior Member, IEEE) was born in India, in 1964. She received the B.Tech. degree in electrical and electronics engineering from Calicut University, in 1986, the M.Tech. degree in lighting science and engineering from Mangalore University, in 1994, and the Ph.D. degree in electrical engineering from Manipal University, Manipal, India, in 2007.

Since 1987, she has been teaching with the Department of Electrical and Electronics Engineering, Manipal Institute of Technology, Manipal, a constituent institution of the Manipal Academy of Higher Education, India. Her research interest includes lighting controls technology and applications.

Dr. Kurian is a Fellow of the Institution of Engineers, India, and a Life Member of professional bodies, including the Indian Society of Lighting Engineers, the Indian Society for Technical Education, and the Systems Society of India.